



## OPEN Enhanced variable step sizes perturb and observe MPPT control to reduce energy loss in photovoltaic systems

Abdelkadir Belhadj Djilali<sup>1</sup>, Elhadj Bounadja<sup>1</sup>, Adil Yahdou<sup>1</sup>, Habib Benboughenni<sup>2✉</sup>, Z. M. S. Elbarbary<sup>3,4</sup>, Ilhami Colak<sup>5</sup> & Saad F. Al-Gahtani<sup>3,4</sup>

This study proposes a modified variable step-size perturb and observe (VSS-P&O) control to improve the efficiency of photovoltaic (PV) systems. Traditional VSS-P&O control often suffers from power losses due to rapid variations in solar irradiance, temperature, and resistive load. The proposed approach enhances the maximum power point tracking technique by incorporating a buck-boost converter to regulate the input and improve tracking accuracy. MATLAB simulations show that the new method significantly outperforms conventional methods, achieving a relative improvement in performance and an 80% reduction in power ripples under varying conditions. Compared to traditional algorithms, the proposed approach reduces response time and undershoots by 30%, demonstrating superior reliability and performance. These findings highlight the effectiveness of the proposed method in addressing power loss issues and improving the overall performance of PV systems, making it a promising solution for future applications.

**Keywords** Buck-boost converter, Photovoltaic system, Maximum power point tracking, Perturb and observe control, Variable step size

### Abbreviations

MPP	Maximum power point
PV	Photovoltaic system
FL	Fuzzy logic
MPPT	Maximum power point tracking
P&O	Perturb and observe control
VSS	Variable step-size
EE	Electrical energy
PSO	Particle swarm optimization
ES	Energy system
FOSC	Fractional-order synergetic controller
PI	Proportional-integral controller
RCC	Ripple correlation control
IC	Incremental conductance
IR	Incremental resistance
REs	Renewable energies
SMC	Sliding mode control
TOSMC	Third-order sliding mode control
FOISMC	Fractional-order integral sliding mode control
SSE	Steady-state error
STC	Super-twisting control

<sup>1</sup>Technology Faculty, Electrical Engineering Department, University of Hassiba Benbouali, Laboratoire de Génie Électrique et Energies Renouvelables (LGEER), Chlef, Algeria. <sup>2</sup>Laboratoire LAAS, Ecole Nationale Polytechnique d'Oran, BP 1523, El M'naouer, Algeria. <sup>3</sup>Department of Electrical Engineering, College of Engineering, King Khalid University, KSA, P.O. Box 394, 61421 Abha, Saudi Arabia. <sup>4</sup>Center for Engineering and Technology Innovations, King Khalid University, 61421 Abha, Saudi Arabia. <sup>5</sup>Department of Electrical and Electronics Engineering, Istinye University, Istanbul, Turkey. ✉email: habib.benboughenni@enp-oran.dz

SVM      Space vector modulation  
 DPC      Direct power control

Currently, the production of electricity is insufficient to meet the increasing consumer demand, prompting researchers to explore various electrical energy (EE) sources<sup>1</sup>. A significant portion of global EE comes from environmentally harmful sources such as gas and oil derivatives, contributing to climate change through pollutant emissions<sup>2</sup>. The use of non-renewable sources increases production and consumption costs, leading to social and economic challenges in non-oil countries. Proposed alternatives include renewable energy sources (RESs) like solar energy (SE)<sup>3</sup>, wind energy (WE)<sup>4</sup>, and sea waves<sup>5</sup>, which are widely available worldwide<sup>6</sup>. These energy systems (ESs) are cost-effective and simple to harness, addressing the rising demand for EE while reducing production and consumption costs<sup>7</sup>. These systems often rely on converting mechanical energy (ME) into EE<sup>8</sup>, reducing the need for electrical lines and protecting the environment and agricultural land<sup>9</sup>. The author believes in the work<sup>10</sup>, that renewable energies (REs) will have a major impact on human life in the future, which requires giving them great importance at present and trying to develop them to achieve the goals sought from their use. According to the work done in<sup>11</sup>, the use of REs allows to significantly reduce the severity of the high demand for EE. Also, the use of these various energy sources allows reducing the costs of producing and consuming EE, which allows economic growth for governments in non-petroleum countries. These sources are many and varied, as several sources can be used together or each source alone to generate EE. In<sup>12</sup>, the author used WE as a source for generating EE, where a multi-rotor wind turbine (MRWT) was used to convert WE into ME. The importance of this ES in the field of EE generation was discussed, as the results showed the effectiveness of the ES and its ability to improve the characteristics of the wind farm. The negative of this ES is that it is expensive and requires regular maintenance as a result of it containing a large number of mechanical components. Relying on MRWT to generate EE will significantly change the concept of ESs, as a single MRWT turbine can be used to supply power to an entire city<sup>13</sup>. Also, the use of MRWT allows to significantly reduce the area of wind farms, which further reduces the cost of producing EE, which is desirable<sup>14</sup>. In<sup>15</sup>, the author used WE along with SE to generate EE. The use of this hybrid ES allows for an increase in energy production and reduces the severity of the use of traditional sources in generating EE, as the use of this ES allows for reducing the phenomenon of global warming. The simulation results showed the effectiveness and high performance of this system under different climatic conditions. This system was discussed in detail in the work done in<sup>16</sup>, where its positives and negatives were mentioned, along with mathematical modeling of each part of it. However, relying on this ES has drawbacks, such as difficulty in control, high costs, and not storing surplus energy, which is negative. In the work<sup>17</sup>, the author used SE to generate EE while storing the surplus energy in batteries. This system is of great importance as it generates and stores energy at the same time. This system was implemented in the MATLAB environment using several scenarios to verify the efficiency of the system. The simulation results showed the extent of its efficacy and effectiveness. However, this system has disadvantages that lie in the high costs of using batteries, as their use increases the costs of the system and the degree of difficulty in controlling it. Also, under difficult weather conditions, there is a large fluctuation in supplying the network with the necessary energy, especially when the duration of bad weather increases and the battery becomes unable to supply the network with the necessary energy. In the work<sup>18</sup>, WE, SE, and a diesel generator (DG) were used to generate EE. This system relies mainly on generating EE using both SE and WE and in difficult weather conditions, a DG is relied upon to compensate for the use of SE and WE in generating EE. Therefore, this system can generate energy in all difficult weather conditions. This ES was tested using MATLAB, and the results showed the effectiveness and importance of this system. Despite this performance, this system has drawbacks that limit its spread, as it is characterized by complexity, high costs, and difficulty in implementation. Also, this ES does not depend on storing surplus energy, which increases energy and financial losses.

Energy quality and costs of energy production are some of the most prominent features that must be focused on in selecting and implementing ESs, as energy quality plays an important role in the effectiveness of the network and the operation of the systems<sup>19</sup>. Therefore, it is necessary to choose an ES based on specifications such as high durability, ease of implementation, fast response time (RT), low costs, ease of control, and reduced use of traditional sources and the spread of toxic gases<sup>20</sup>. The author believes in the work<sup>21</sup> that the control approach has a major role in increasing system durability, and power quality, and reducing costs. Therefore, in this work, a simple ES is proposed that relies on the use of SE to generate EE, while using a control approach characterized by high performance and great durability.

The photovoltaic (PV) system is one of the most important systems proposed and used for generating EE due to several features that make it different from other systems<sup>22</sup>. This system relies on the use of PV cells in the form of panels, as they are characterized by simplicity, inexpensive, and easy to manufacture, which allows their use to reduce the costs of production and consumption of EE. Also, using a PV system helps reduce toxic gas emissions and protects the environment from pollution, which is desirable. This system is easy to use and does not require large areas, as solar panels can be placed on the roofs of houses, allowing for reducing production costs and EE consumption. Compared to WTs, PV systems based on SE are considered one of the most prominent ESs due to their ease of operation, availability of SE year-round, environmental friendliness, and cost-effectiveness<sup>23</sup>. This study focuses on generating EE from PV systems, with particular emphasis on the control approach.

As is known, PV systems operate silently compared to WE systems that cause noise, and this feature makes this system widespread and desirable<sup>24</sup>. This system can be used in street lighting, water pumping, and electric vehicles, and can be integrated into hybrid ES modules. However, PV cells have relatively low conversion efficiencies (15–30%) compared to other energy sources. Maximum power point (MPP) tracking (MPPT) strategy is a technology used to control a PV system<sup>25</sup>. This approach is characterized by simplicity, inexpensive, easy to use and apply, and its use does not require knowledge of the mathematical model of the system<sup>26</sup>.

Various MPPT approaches have been developed, such as Hill-climbing<sup>27</sup>, neural networks<sup>28</sup>, fractional short circuit current<sup>29</sup>, fractional open-circuit voltage<sup>30</sup>, incremental conductance (IC)<sup>31</sup>, perturb and observe (P&O)<sup>32</sup>, fuzzy logic (FL) control<sup>33</sup>, particle swarm optimization (PSO) algorithm<sup>34</sup>, backstepping control (BC) strategy<sup>35</sup>, incremental resistance (IR)<sup>36</sup>, and ripple correlation control (RCC)<sup>37</sup>. Among these, the P&O technique has gained significant attention but faces challenges with power loss during rapid changes in atmospheric conditions, as highlighted in previous studies<sup>38</sup>. To address this, solutions incorporating changes in current ( $\Delta I$ ), power ( $\Delta P$ ), and voltage ( $\Delta V$ ) have been proposed<sup>39</sup>. Modifications such as a modified P&O algorithm<sup>40</sup>, a PSO-based neuro-fuzzy approach<sup>41</sup>, and a crow search algorithm<sup>42</sup> have been suggested. Additionally, in<sup>43</sup>, the author introduced a novel MPPT model for PV systems using a nonlinear approach known as the neural BC approach. This modified approach is renowned for its robustness, high competence, simplicity, and ease of implementation. MATLAB simulations confirmed that the MPPT technique based on the neural BC approach outperforms the traditional approach in terms of performance, robustness, steady-state error (SSE), overshoot, and power quality. Neural networks are combined with sliding mode control in<sup>44</sup> to obtain a strategy that can overcome the problems of the MPPT approach of PV system. The proposed strategy is compared with the MPPT-P&O technique, MPPT-FL strategy, and MPPT strategy based on the neural proportional-integral (PI) controller. The proposed strategy is implemented in a MATLAB environment, where the obtained results show the efficiency and effectiveness of the proposed approach in improving the characteristics of the PV system compared to other strategies in terms of improving the quality of power and current. In<sup>45</sup>, the crow search algorithm was used to improve the MPPT strategy characteristics of the PV system. This strategy is characterized by simplicity, ease of implementation, low cost, and excellent performance. The results showed that using the crow search algorithm outperforms the traditional approach in terms of improving the quality of power and current.

The double integral sliding mode approach is the solution proposed in<sup>46</sup> to improve the characteristics of the MPPT strategy of the PV system. This strategy differs from the traditional strategy in terms of principle, durability, performance, and results provided. Simulation and experimental work were used to ensure the robustness and effectiveness of the proposed strategy while comparing the results with the traditional strategy. The proposed approach reduced the energy ripples and SSE value significantly compared to the conventional approach. Using the double integral sliding mode in the strategy creates the problem of chattering, which is an undesirable negative. A new MPPT strategy is proposed in<sup>47</sup> based on the use of the bacterial foraging optimization (BFO) algorithm to increase the performance. This proposed strategy is used to control the DC-link capacitor voltage of a solar PV converter. The use of this proposed strategy allows for optimal control of active and reactive power. MATLAB was used to implement the MPPT-BFO strategy based on different scenarios. The simulation results showed that the overshoot and settling time values in the case without solar-PV inverter were 44.32% and 5.2 s, respectively. In the case with solar-PV inverter, the settling time and overshoot values were estimated to be 3.02 s and 7.66%, respectively. In the case with the MPPT-BFO-based solar-PV inverter, the overshoot and settling time values were estimated to be 3.88% and 1.1 s, respectively. Therefore, using the MPPT-BFO strategy leads to a significant improvement in the values of both settling time and overshoot. Also, the results showed that the power quality is higher in the case of using the MPPT-BFO strategy compared to the conventional approach. Bacterial swarm optimization (BSO) algorithm is proposed in<sup>48</sup> to overcome the drawbacks of the MPPT strategy of PV-STATCOM (Static synchronous compensator). This proposed strategy is different from the traditional strategy. The proposed strategy is characterized by high robustness, excellent performance, easy implementation, and low cost. Using this proposed strategy does not require knowing the mathematical model of the system under study accurately, which gives this strategy an advantage in case the machine parameters change compared to the traditional approach. MATLAB was used to implement and verify the efficiency of this proposed strategy, comparing the results with the traditional MPPT approach. The simulation results show that the MPPT-BSO approach improves the overshoot and settling time by 82.53% and 70.28%, respectively, compared to the conventional approach. These improvements make the MPPT-BSO approach interesting for other energy applications. In<sup>49</sup>, a comparison of three smart strategies is proposed to find out the best strategy that has the greatest efficiency in improving the MPPT of PV-plant operates as VSC (Voltage Source Converter)-STATCOM (Static synchronous compensator). These three smart strategies are the PSO algorithm, the BFOA (Bacterial foraging optimization algorithm), and the hybrid PSO-BFOA. These proposed strategies were used to mitigate and control the power fluctuations of a PV farm. MATLAB was used to implement these proposed strategies, and the simulation results showed that the MPPT strategy of the PV system based on the hybrid PSO-BFOA algorithm is superior in terms of mitigating the power fluctuations and improving the dynamic response of the output power of the PV system.

Despite the promising results, there are drawbacks to the designed approaches. These include power and current ripples, which are undesirable. In<sup>50</sup>, a fractional-order integral SMC (FOISM) was used to control a three-phase grid-connected PV inverter. The system simultaneously generates and filters energy, making it significant in the energy field. The FOISM strategy was used alongside a PSO approach for gain estimation, leading to satisfactory results. The approach outperformed conventional PI regulators in terms of performance, robustness, and competence. In<sup>51</sup>, the author proposed a super-twisting control (STC) based on a genetic algorithm (GA) to improve both direct power control (DPC) and MPPT of PV systems. This method is simple, inexpensive, and model-independent, with a notable reduction in total harmonic distortion and power fluctuations. The approach also improved the DC link voltage and overall system stability.

An enhanced Beetle Antenna Search (e-BAS) was used in<sup>52</sup> to control a solar PV system. This approach provided high robustness and efficiency without requiring a model of the ES, showing superiority over traditional methods in terms of power quality and reducing energy fluctuations. In the work<sup>53</sup>, it was proposed to use coordinated voltage control to improve the characteristics of the PV system. This work aims to reduce energy loss while keeping the voltage within reasonable limits, where a discrete jellyfish search algorithm was presented to calculate the gain values of the proposed approach and to achieve the best results. Simulation was used to

verify the effectiveness and efficiency of the proposed approach in improving power quality, where several different tests were used. Simulation results show that the proposed approach significantly reduces energy usage as well as losses and voltage variation.

Other nonlinear controllers, such as a simplified STC<sup>54</sup>, and an integral robust nonlinear BC approach<sup>55</sup>, have also been designed to improve the MPPT strategy and DPC technique. These controllers are characterized by simplicity, robustness, and high efficiency, though they face challenges related to complexity and the number of parameters required for tuning. In<sup>56</sup>, a synergetic control (SC) approach was highlighted as improving system robustness and dynamic response compared to conventional PI controllers. The use of fractional-order SC (FOSC) strategy further enhanced power and current quality, though power fluctuation issues persist. In<sup>57</sup>, the author combined supervised learning and deep reinforcement learning techniques to improve the characteristics of the PV system. This strategy is characterized by high performance and great effectiveness in improving power quality, and this is shown by the simulation results compared to the traditional strategy. Also, using this suggested approach helps track the global MPP, which is positive. The predictive control approach<sup>58</sup> was suggested to improve system durability and reduce errors, though its complexity and cost remain a concern.

In conclusion, the key challenge in PV system control lies in selecting the appropriate control strategy to enhance system performance and power quality. This underscores the need for further research into simpler yet efficient solutions that balance robustness, simplicity, and cost-effectiveness.

Existing MPPT approaches for PV systems, such as fixed-step P&O strategy, variable step-size P&O (VSS-P&O) strategy, and heuristic techniques like the PSO approach and FL strategy, have shown significant limitations. These include energy loss during rapid environmental changes, slow response time, and computational complexity. Addressing these challenges, this paper proposes a modified VSS-P&O algorithm designed to enhance the MPPT strategy process. The proposed method offers improved energy efficiency, faster RT, and simplicity in implementation, making it a robust solution for minimizing energy loss under dynamic operating conditions. The results demonstrate its superiority over conventional methods in terms of reduced energy loss, faster tracking, and enhanced stability.

A critical review of existing literature reveals that existing solutions for power loss optimization in PV systems yield unsatisfactory results. To address this, the paper proposes an innovative approach to minimize power loss during rapid changes in solar irradiation (SI), temperature ( $T$ ), and resistive load ( $RL$ ). The proposed method incorporates derivative functions ( $\Delta G/\Delta t$ ,  $\Delta T/\Delta t$ ,  $\Delta RL/\Delta t$ ) and changes in SI ( $\Delta G$ ),  $T$  ( $\Delta T$ ),  $RL$  ( $\Delta RL$ ), power ( $\Delta P$ ), and voltage ( $\Delta V$ ) within a modified VSS for the MPPT-P&O technique. The proposed MPPT-P&O approach based on modified VSS is a modification and development of the MPPT-P&O technique. Simplicity, ease of realization, high performance, great robustness, and effectiveness in improving the characteristics of the system under study are among the most prominent features of the proposed approach. The primary objective of this study is to develop a robust and efficient modified VSS-P&O algorithm tailored to enhance the MPPT strategy of PV systems. The proposed approach addresses the challenge of energy loss during rapid variations in solar irradiance, temperature, and resistive load by integrating derivative functions and adaptive decision-making processes. This method significantly improves system responsiveness by reducing RT, undershoot, and power ripples, thereby ensuring faster dynamic performance and greater stability compared to traditional techniques. The study also focuses on maximizing solar energy utilization and minimizing energy losses, contributing to improved sustainability and reduced dependence on non-RESs. The effectiveness of the algorithm is rigorously validated through MATLAB simulations under varying environmental and load conditions, demonstrating superior performance metrics such as higher efficiency, reduced energy drift, and enhanced robustness. Additionally, the study establishes a scalable framework for future enhancements, including its potential application in hybrid systems and under partial shading conditions, paving the way for further advancements in the field of RE systems.

Therefore, the MPPT-P&O approach based on modified VSS is the main contribution of this paper. Developing an effective strategy for responding rapidly to changes in SI,  $T$ , and load is a significant challenge in SE. The proposed approach overcomes this by creating models and ESs that adapt quickly to environmental variables and operating conditions. The proposed strategy was implemented in the MATLAB environment, comparing the performance and efficiency with the traditional strategy, where several different tests were used to study the performance of the proposed approach. The objectives achieved from this completed work can be identified in the following points:

- Enhanced variable step size perturbation: The step size perturbation is finely tuned to adjust to rapid environmental changes, ensuring maximum SE conversion efficiency without oscillations.
- Accurate data reading and decision-making: The approach ensures precise data collection, which is crucial for making fact-based decisions and optimizing MPPT performance.
- Improved SE utilization and reduced losses: By increasing the efficiency of SE usage, the method minimizes losses, thereby improving sustainability and maximizing RE utilization.
- Significant progress in the SE field: This method contributes to advancing PV systems, offering the potential for wide application to enhance their role in RE.

In addition to the above-mentioned goals, using the proposed approach allows for improving the dynamic power response compared to the traditional approach. Moreover, its use leads to a reduction in both ripples and the undershoot value of power compared to traditional techniques.

In conclusion, the proposed approach significantly improves PV system efficiency, helping reduce reliance on environmentally harmful energy sources and mitigating harmful emissions.

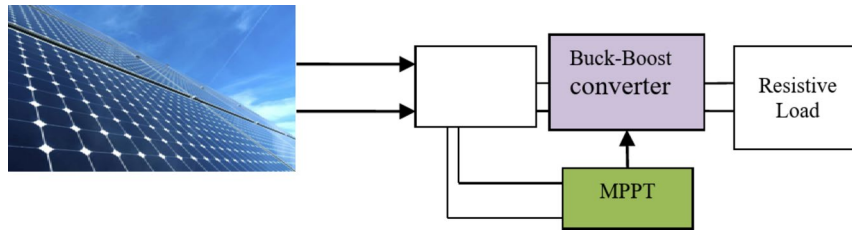


**Fig. 1.** PV system.

Parameter	Value
$C_2$	560 $\mu$ F
$C_1$	560 $\mu$ F
$L$	350 $\mu$ H

**Table 1.** DC-DC-BBC parameters.

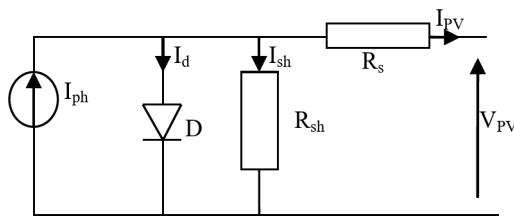


**Fig. 2.** PV cell model. Where,  $R_s$ : Series resistance of the PV module;  $I_{ph}$ : PV stream source;  $D$ : Diode connected in parallel;  $V_{PV}$ : PV voltage;  $R_{sh}$ : Shunt resistance;  $I_{PV}$ : Difference between the photocurrent  $I_{ph}$  and the diode stream  $I_d$  and  $I_{sh}$  which is given by Eq. (1).

The structure of the article is as follows: section “[PV system and its model](#)” presents the PV system and its model, section “[Modified VSS-P&O approach](#)” modifies the VSS-P&O approach, section “[Simulation analysis](#)” introduces the simulation analysis, and section “[Conclusions](#)” concludes with the main contributions.

### PV system and its model

The ES arrangement depicted in Fig. 1 aims to regulate the MPP of the PV module and steer the ES towards an operational point near the MPPT technique<sup>59</sup>. This proposed system is simple, inexpensive, easy to implement, and low maintenance. Relying on this system allows for the reduction of dependence on traditional energies and thus protects the environment, which is a good thing. This system can be used on the roofs of buildings, allowing the reduction of SE farms. The power output from this system changes depending on the change in SI,  $T$ , and the resistive load.

The PV module’s output is linked to a DC-DC buck-boost converter (DC-DC-BBC), a crucial element in the operation of the MPPT technique. The specifications for the DC-DC-BBC component are detailed in Table 1. The MPPT technique manages the duty cycle ( $D$ ) of the DC-DC-BBC to attain MPP. The system’s output is connected to both a fixed (10  $\Omega$ ) and a variable resistive load (Ranging from 5  $\Omega$  to 8  $\Omega$  and then from 8  $\Omega$  to 5  $\Omega$ ).

### PV model

The PV system is one of the simplest ESs that has been used in recent years due to its low cost and ease of maintenance<sup>60</sup>, as its use does not require complex technology. This system relies on solar cells similar to a diode with a PN connection, as these cells work when exposed to the sun to convert this light ray into an electric current<sup>61</sup>. To obtain the necessary energy, several solar panels must be used. According to the work done in<sup>62</sup>, controlling the PV system is simple and does not require the use of complex strategies, as the MPPT strategy can be used for this purpose. Despite the advantages of this system and its high ability to mitigate the severity of global warming and the high energy demand, it is characterized by drawbacks that limit its spread, such as energy ripples and fluctuations in EE production in difficult weather conditions. The mathematical model for a PV cell is simple, and this model was discussed in detail in the work done in<sup>63</sup>. This model of a PV cell is represented in Fig. 2.

$$I_{PV} = I_{ph} - I_d - I_{sh} \tag{1}$$

$$I_{PV} = I_{ph} - I_o \left[ \exp \left( \frac{qV_{PV} + qR_s I_{PV}}{N_s K T a} \right) - 1 \right] - \frac{V_{PV} + R_s I_{PV}}{R_{sh}} \tag{2}$$

$I_o$  is the saturation stream,  $K$  is Boltzmann's constant ( $1.38 \times 10^{-23}$  J/K),  $q$  is charge of an electron ( $1.6 \times 10^{-19}$  C),  $a$  is diode ideality factor, and  $N_s$  is the number of cells in series.

$I_{ph}$  is expressed as,

$$I_{ph} = [I_{SC} + K_{SC} (T - 298)] \frac{G}{G_{SC}} \tag{3}$$

where,  $I_{sc}$  is the short-circuit stream at standard test conditions,  $G$  ( $W/m^2$ ) is the SI on the cell surface, and  $K_{sc}$  is the short circuit stream coefficient.

$I_o$  is influenced by the temperature according to the following equation,

$$I_o = \frac{I_{SC} + K_{SC} (T - 298)}{\exp [V_{OC} + K_V (T - 298) / a \times V_{th}] - 1} \tag{4}$$

$V_{th}$  is the thermal voltage of the cell, which is expressed as,

$$V_{th} = (K \times T) / q \tag{5}$$

### DC-DC-BBC model

The DC-DC-BBC in the studied PS functions as a buck-boost chopper, serving as an impedance adaptor. By adjusting the  $D$ , it aligns its input impedance with that of the PV module to achieve MPPT technique. Figure 3 represents the architecture of the DC-DC-BBC used in this paper. Component specifications are listed in Table 1. The MPPT technique is realized by measuring the PV module's electrical parameters and using an MPPT controller to drive  $D$ <sup>64</sup>.

Equation (6) represents the input and output voltages. Using Eq. (6), the ratio of Output voltage from the converter to Input voltage to the converter is calculated. This ratio is related to the Duty cycle.

$$\frac{V_L}{V_{PV}} = \frac{D}{1 - D} \tag{6}$$

where,  $V_{PV}$ : Input voltage to the converter,  $V_L$ : Output voltage from the converter,  $D$ : Duty cycle.

Equation (7) represents input–output powers.

$$P_{PV} = P_L \tag{7}$$

With:

$$V_{PV} \times I_{PV} = V_L \times I_L \tag{8}$$

$$\frac{V_L}{V_{PV}} = \frac{I_{PV}}{I_L} \tag{9}$$

where,  $I_{PV}$ : Input current to the converter,  $I_L$ : Output current from the converter.

$$\frac{I_{PV}}{I_L} = \frac{D}{1 - D} \tag{10}$$

The input impedance ( $R_{in}$ ) can be expressed as:

$$R_{in} = \frac{V_{PV}}{I_{PV}} \tag{11}$$

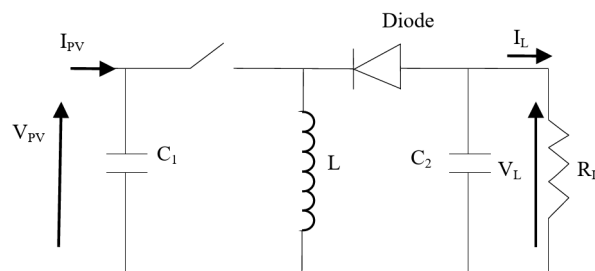


Fig. 3. DC-DC-BBC model.

Substituting Eqs. (6) and (10) into Eq. (11), the DC-DC-BBC input impedance can be expressed as:

$$R_{in} = \frac{(1 - D)^2}{D^2} \times \frac{V_L}{I_L} = \frac{(1 - D)^2}{D^2} \times R_L \tag{12}$$

From Eq. (12), this can be seen by changing  $D$ , the value of  $R_{in}$  can be varied and matched with the optimal input impedance ( $R_{opt}$ ) of the PV panel at the MPP for  $R_L$ , where:

$$R_{opt} = \frac{V_{MPP}}{I_{MPP}} \tag{13}$$

Switching transients in the buck-boost converter introduces voltage and current fluctuations, leading to increased energy losses and potential stability issues. High-frequency switching events generate transient spikes that can impact the converter’s efficiency and reliability. The proposed control method addresses these issues by incorporating an adaptive step-size mechanism that dynamically adjusts the duty cycle to mitigate transient oscillations. This ensures smoother voltage regulation and reduces power losses associated with abrupt switching transitions.

**Conventional variable step size P&O control**

The VSS-P&O is a variant of the P&O algorithm, where the step size is automatically adjusted for fast and accurate tracking<sup>65</sup>. A large perturbation improves dynamic performance, while smaller values enhance steady-state accuracy. The  $D$  with adaptive step size is defined as follows<sup>66</sup>.

$$\Delta D_{VSS} = \pm M \times |P(t) - P(t - 1)| / V(t) - V(t - 1) \tag{14}$$

where,  $M$  is the scaling factor, tuned during design. Power loss affects the VSS-P&O algorithm more significantly under rapid changes in SI due to the large perturbation value. Figure 4 illustrates the VSS-P&O algorithm.

In this work, the duty cycle  $D$  plays a central role in controlling the input–output behavior of the DC-DC buck-boost converter. While Eq. (6) provides the fundamental relationship between the input voltage ( $V_{PV}$ ) and the output voltage ( $V_L$ ), the dynamic adjustment of  $D$  is influenced by the  $\Delta VSS$ . The perturbation size  $\Delta VSS$  dynamically adapts based on the proximity of the operating point to the MPP: larger perturbations ensure faster convergence when far from the MPP, while smaller perturbations enhance accuracy near the MPP, minimizing oscillations. This adaptive adjustment indirectly modifies  $D$ , ensuring optimal tracking of the MPP under varying environmental conditions. Consequently,  $\Delta VSS$  is a critical factor influencing the efficiency and accuracy of the MPPT algorithm, even though it does not explicitly appear in Eq. (6).

In this study, the PV panel was tested under three scenarios:

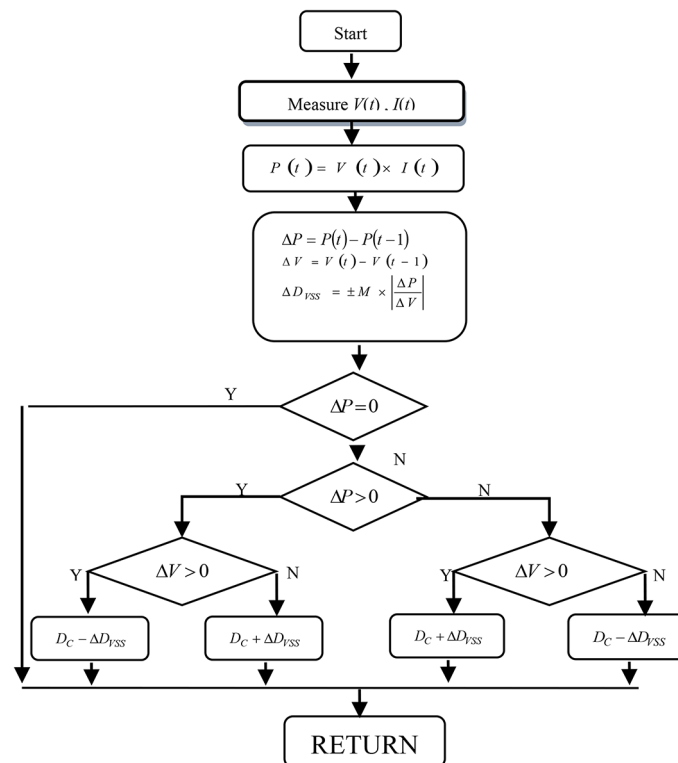


Fig. 4. Traditional VSS-P&O approach.

1. The rapid change in SI, with  $T$  and resistive load, held constant.
2. The rapid change in  $T$ , with SI and resistive load, held constant.
3. The rapid change in resistive load, with SI and  $T$ , held constant.

Figure 5 shows the three scenarios applied to the PV panel. In the first case, the  $T$  value is fixed at 25 °C, and the resistive load value is set at 10 ohms. Also, the SI value changes upward from 600 W/m<sup>2</sup>, then 800 W/m<sup>2</sup>, then 1000 W/m<sup>2</sup> during periods 0 s, 3 s, and 6 s, respectively.

In the second case, the SI value is fixed at 1000 W/m<sup>2</sup> and the resistive load value is fixed at 10 ohms. Also, the reduction of the value of  $T$  is changed from 48 to 46 °C at the time point of 5 s. The value of  $T$  is raised from 35 to 45 °C at the time point of 5 s. In the third case, the values of SI and  $T$  are fixed at 1000 W/m<sup>2</sup> and 25 °C, respectively. Also, the resistive load is changed by ascending from 5 to 8 ohms at the 3-s time point and the resistive load value is changed by descending from 8 to 2 ohms at the 3-s time point.

### Power loss problem analysis

#### Power loss problem analysis during rapid change of SI

In Fig. 6, it is observed that the VSS-P&O causes power loss during rapid changes in solar irradiance (SI). Figure 7 provides a detailed explanation of this issue. When the SI is 600 W/m<sup>2</sup>, the power is 37.53 W. However, when the SI rapidly increases from 600 to 800 W/m<sup>2</sup>, point 1 (37.53 W) shifts to point 2, then to point 4 (34.91 W), instead of reaching point 3 (50 W), resulting in power loss. Similarly, when the SI suddenly rises from 800 to 1000 W/m<sup>2</sup>, point 3 (50 W) moves to point 5, then to point 7 (43.22 W). This issue arises due to errors in the MPPT tracking direction, as VSS-P&O relies on  $\Delta V$  and  $\Delta P$ , which provide inaccurate information during rapid SI changes, leading to power loss.

At point 1 the voltage is equal to 20.38 V and the energy is 37.53 W, and when the SI changed rapidly, point 1 moving to point 2 (20.95 V, 49.39 W), this means that the change is:

$$\begin{cases} \Delta V = 20.95 - 20.38 = 0.578 \text{ V}, & \Delta V > 0 \\ \Delta P = 49.38 - 37.53 = 11.86 \text{ W}, & \Delta P > 0 \end{cases}$$

Because  $(\Delta P / \Delta V) > 0$  the VSS-P&O algorithm thinks it is still moving in the same direction to find the MPP, it maintains a large and negative VSS perturbation ( $\Delta D_{VSS} = -M \times |\Delta P / \Delta V|$ ) and this is what causes the energy loss problem.

Figure 8 shows the problem of energy loss when rapidly decreasing in the level of SI.

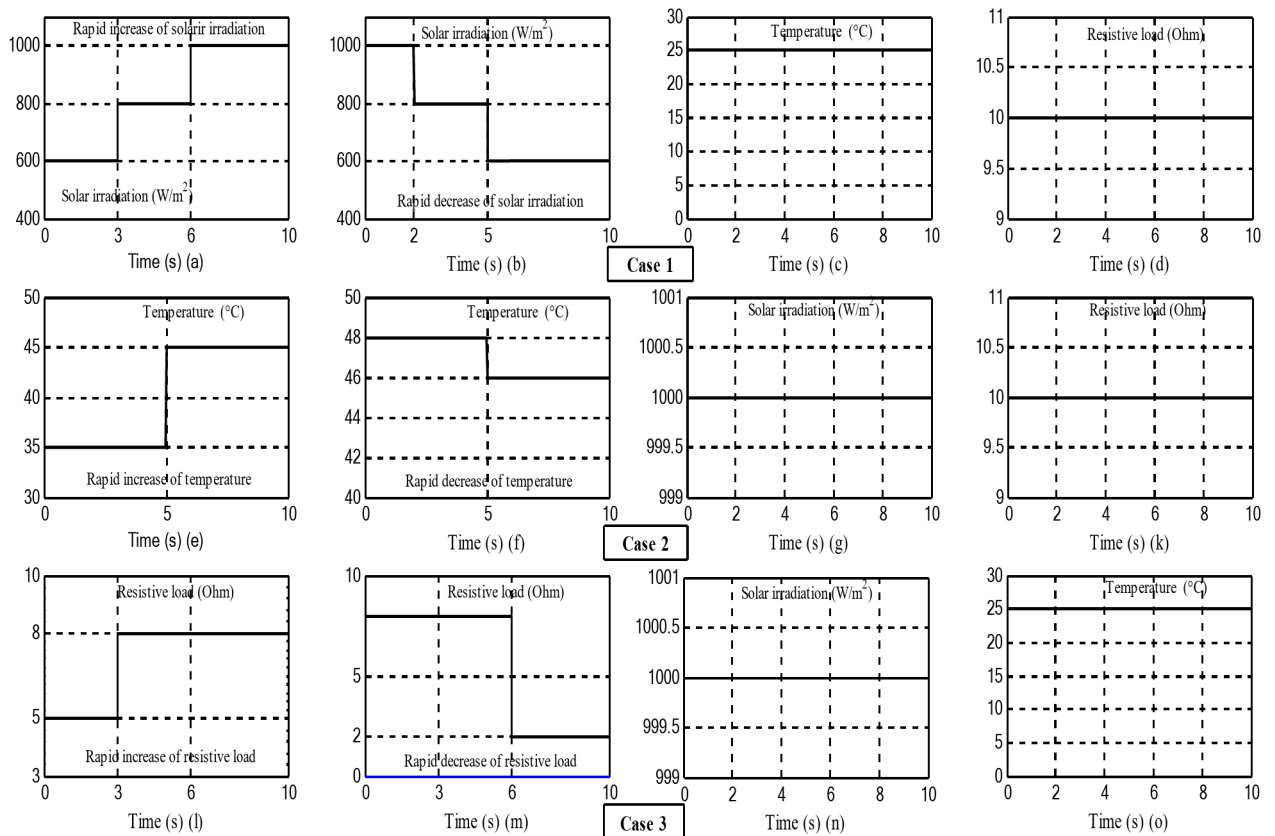
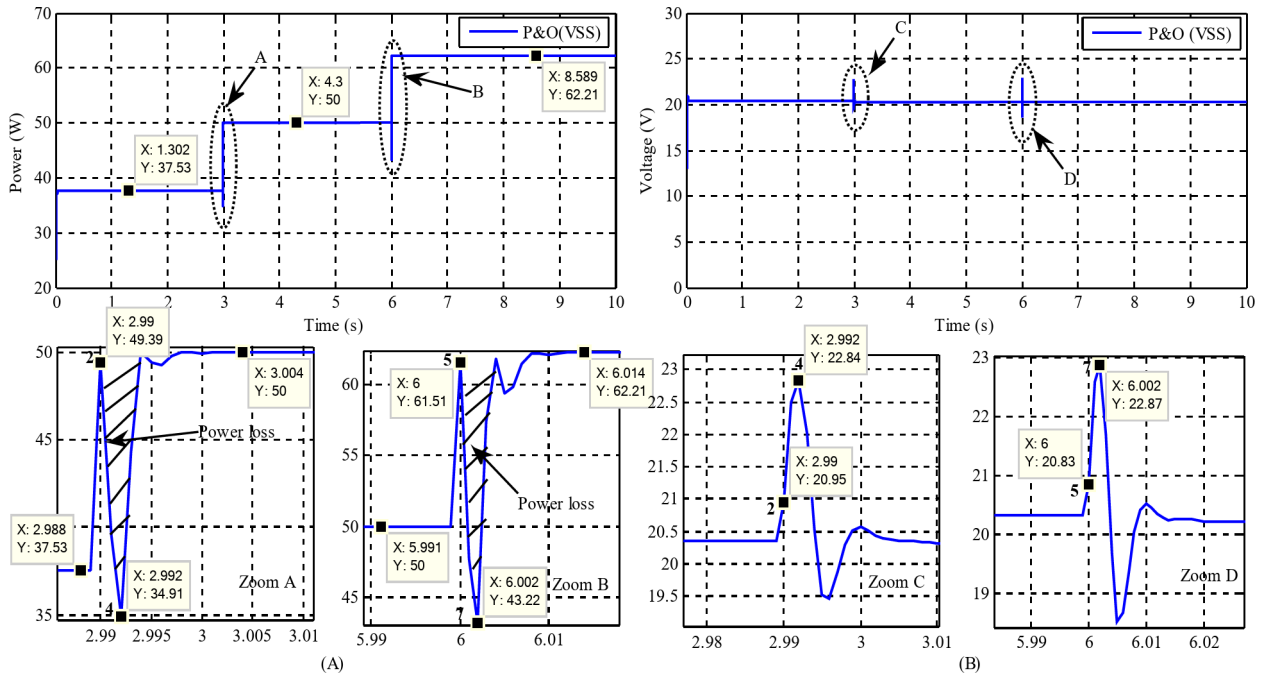
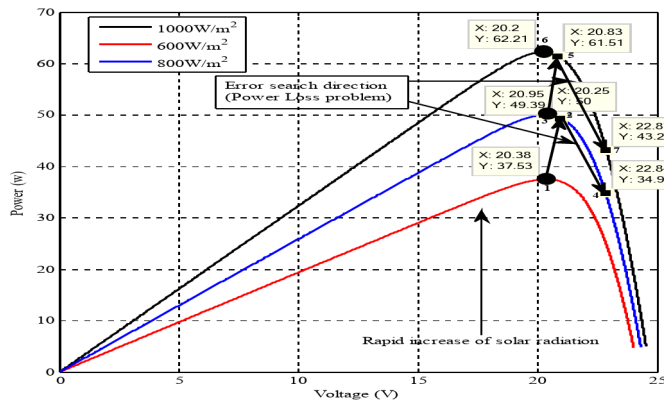


Fig. 5. Different cases of atmospheric conditions.



**Fig. 6.** (a) Power loss problem during increase of SI and (b) PV module output voltage using VSS-P&O during increase of SI.



**Fig. 7.** Power loss problem during rapid increase of SI.

It is observed from Fig. 8b that when a rapid decrease in SI occurs, point A (20.24 V, 62.21 W) from the first level curve (1000 W/m<sup>2</sup>) moves to point B (19.69 V, 49.58 W) from the second level curve (800 W/m<sup>2</sup>) near the MPP ( $P_{max}$ ). This change generates the following:

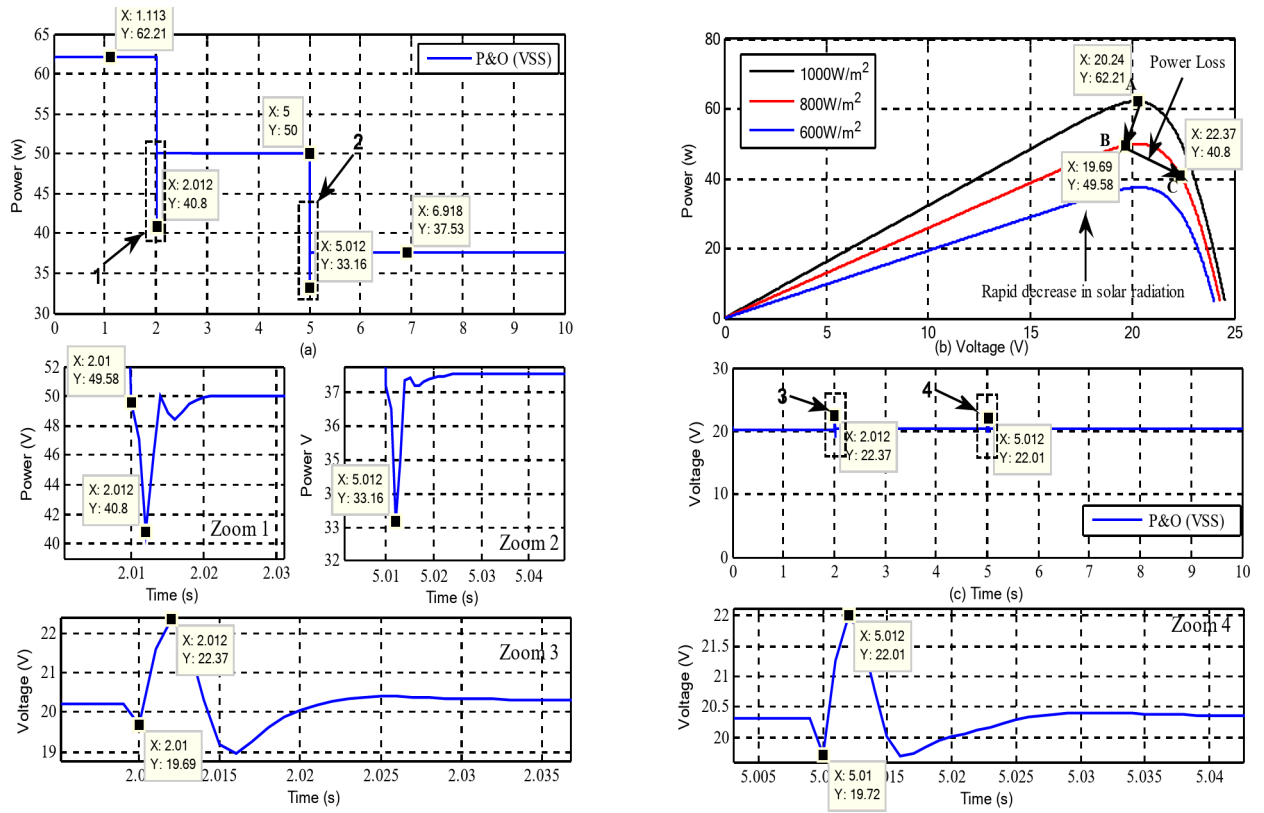
$$\begin{cases} \Delta V = 19.69 - 20.24 = -0.55V, \Delta V < 0 \\ \Delta P = 49.58 - 62.21 = -12.63w, \Delta P < 0 \end{cases}$$

In this case, the VSS-P&O algorithm takes the right direction search to make  $\Delta D_{VSS}$  negative, but the rapid change in SI causes it to make a wrong decision and this gives it a large step size perturbation  $\Delta D_{VSS}$  (shows Figs. 9 and 10) which causes the transition to point C (22.37 V, 40.9 W) far to  $P_{max}$  causing energy loss problem.

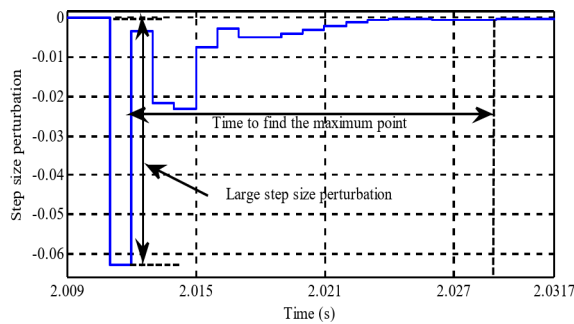
*Power loss problem analysis during rapid change of T*

Figure 11 illustrates the problem of energy loss when rapidly decreasing in T. The T change from high (48 °C) to low (46 °C) increases the output energy of the PV panel as shown in Fig. 11a. The rapid change in T causes the problem of energy loss, as shown in Fig. 11b1.

At T= 48 °C, the MPP on the PV curve (Fig. 11c) is at point A (18.78 V, 58.01 W). When T rapidly decreases to 46 °C, point A moves to a higher PV curve, reaching point B (18.79 V, 58.36 W), away from the original maximum point.



**Fig. 8.** (a) Power loss problem during decrease of SI and (b) PV curve during rapid decrease of SI, (c) PV module output voltage using VSS-P&O in decrease of SI.



**Fig. 9.** Step size perturbation waveform of VSS-P&O during rapid decrease of SI (1000 W/m<sup>2</sup> to 800 W/m<sup>2</sup>).

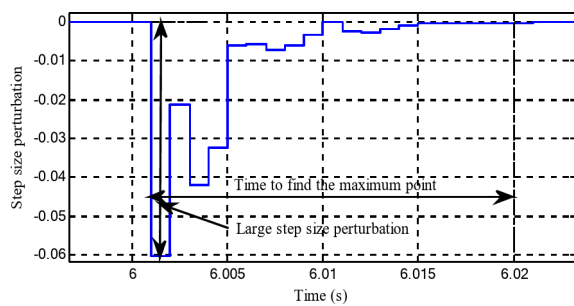


**Fig. 10.** Step size perturbation waveform of VSS-P&O during rapid increase of SI (800 W/m<sup>2</sup> to 1000 W/m<sup>2</sup>).

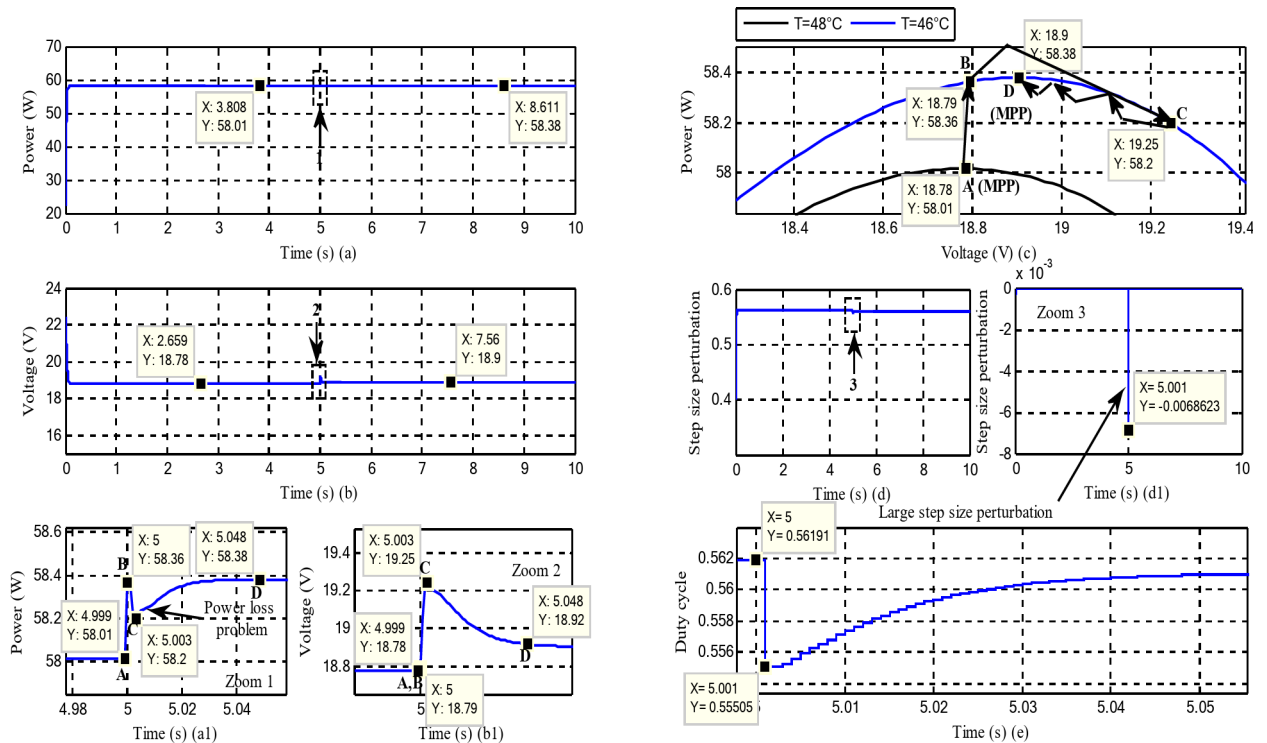


**Fig. 11.** (a) Power loss problem during decrease of  $T$ , (b) PV module output voltage in decrease of  $T$ , (c) PV curve during rapid decrease of  $T$ , (d) Step size perturbation during rapid decrease of  $T$ , and (e)  $D$  during rapid decrease of  $T$ .

$$\text{At point B: } \begin{cases} \Delta V = 18.79 - 18.78 = 0.01 \text{ V}, & \Delta V > 0 \\ \Delta P = 58.36 - 58.01 = 0.35 \text{ W}, & \Delta P > 0 \end{cases}$$

At this moment, VSS-P&O technique moves in the correct search direction, but the rapid change in  $T$  causes an incorrect decision, resulting in a large step-size perturbation (as shown in Fig. 11d1). This shifts point B to point C (19.25 V, 58.2 W), which is far from  $P_{\max}$ , causing energy loss.

At  $t = 5$  s at point C ( $\Delta V > 0, \Delta P < 0$ ) the VSS-P&O decreases  $D$  significantly using a large VSS perturbation (Fig. 11e), moving point B to point C, far from point D (MPPT), which caused energy loss.

Applying the same method, when the PV panel experiences a rapid temperature increase (from 35 °C to 45 °C), the results shown in Fig. 12 are obtained.

It is observed from Fig. 12 that when a rapid increase in  $T$  occurs from 35 °C to 45 °C, the maximum point A (19.59 V, 60.39 W) located on the higher PV characteristic curve moves to point B (19.49 V, 58.11 W) of the lower PV feature curve to the left of the new operating point D (18.97 V, 58.57 W), at this moment the information is ( $\Delta V < 0, \Delta P < 0$ ) and the VSS-P&O algorithm decreasing the  $D$  by a big VSS perturbation, which makes point B moves to point C (19.79 V, 57.37 W) away from operating point D, this error causes the problem of energy loss.

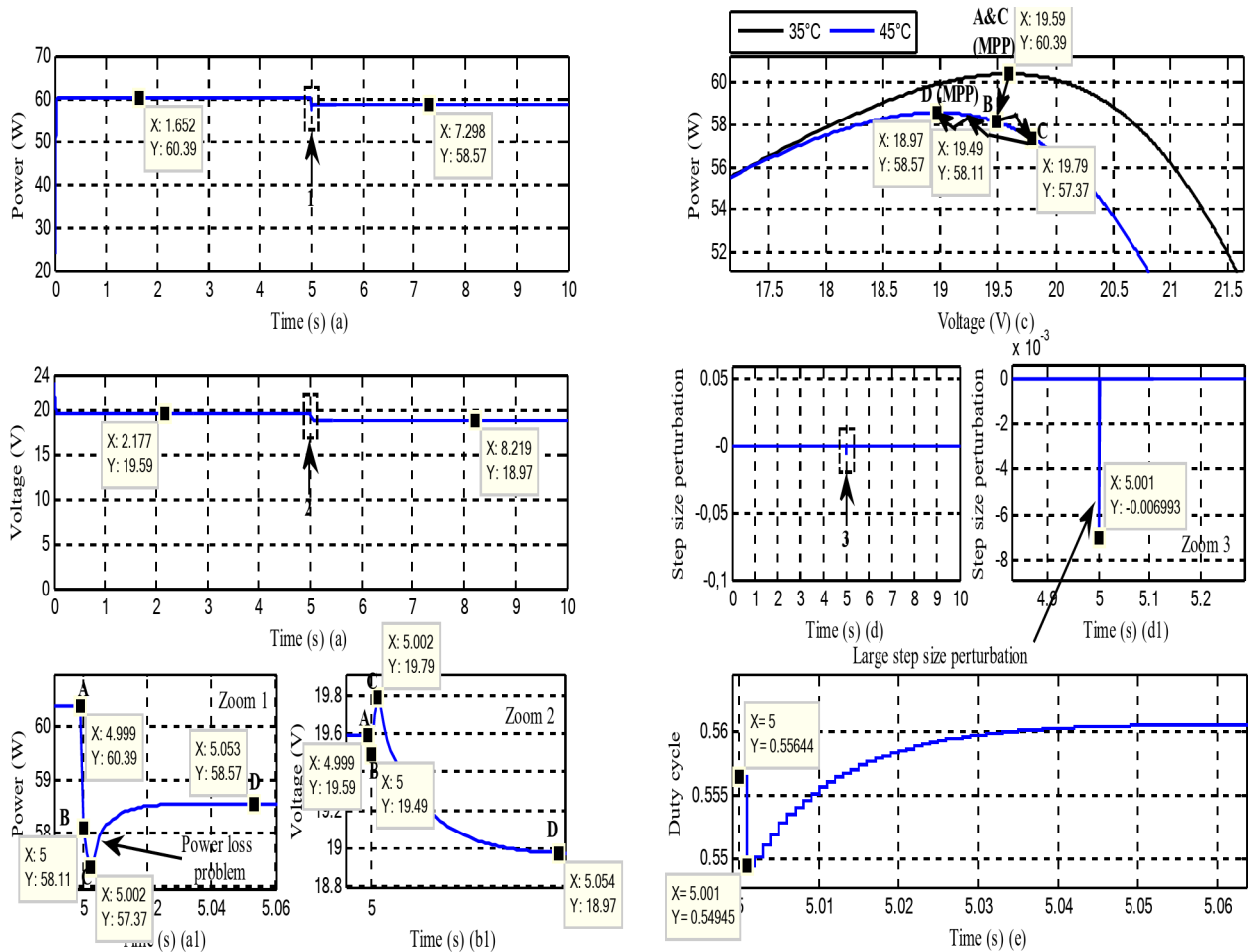
*Power loss problem analysis during rapid change of resistive load*

Figure 13 represents the waveform, at STC algorithm ( $G = 1000 \text{ W/m}^2, T = 25 \text{ }^\circ\text{C}$ ), in rapid increase of resistive load (shown in case 3 of Fig. 5a1). Initially, the load resistance is set to  $R = 5 \text{ } \Omega$ , which is lower than the optimal resistance ( $R_{\text{opt}} = 6.552 \text{ } \Omega$ ). At  $t = 3$  s, it rapidly increases to  $R = 8 \text{ } \Omega$ . At  $t = 3$  s when a rapid resistive load exists, the operating MPP A (20.22 V, 62.21 W) as presented in Fig. 13c moves to point B (22.21 V, 52.43 W).

At point B, the P&O-VSS algorithm detects this change. To return to the operating point, the  $D$  must be adjusted to its optimal value,  $D_{\text{opt}}$ .

P&O-VSS algorithm increases the  $D$  by a variable small step size as depicted in Fig. 13e and moves point B to point C (MPPT) slowly, and then causes the occurrence of the energy loss problem as shown in Fig. 13a1.

Figure 14 illustrates the power loss problem during the rapid increase of resistive load. At point B the P&O-VSS technique detected that  $\Delta V < 0$  and  $\Delta P < 0$ , at this moment P&O-VSS technique decreased the  $D$  by a variable small step size as shown in Fig. 14e. The slow speed research due to small step size perturbation moves point B to point C (MPPT) quickly then causing the Energy loss problem as shown in Fig. 14a1.



**Fig. 12.** (a) Power loss problem during increase of  $T$ , (b) PV module output voltage in increase of  $T$ , (c) PV curve during rapid increase of  $T$ , (d) Step size perturbation during rapid increase of  $T$ , and (e)  $D$  during rapid increase of  $T$ .

### Modified VSS-P&O approach

The rapid change of SI, temperature, and resistive load causes the VSS-P&O technique to make the wrong decisions to extract the MPP (loss power problem), these wrong decisions are the error of search direction to find a MPPT technique and the error in the step size perturbation (large value in the case of rapid change of SI and  $T$  and small value in the case of rapid change of resistive load).

### Solution method during the rapid change of SI

Figure 15 illustrates the MPPT method under a rapid increase in solar irradiation (SI). Figure 15a, c show that when a sudden increase in SI occurs, point A jumps to point B, which is near point C (MPPT technique). However, it then moves directly to point D, far from C. This behavior is due to the information obtained by the VSS-P&O method. Because the step size is large, point B moves to D, which is far from C (MPPT technique).

To overcome this drawback, a modified VSS-P&O technique was implemented. The results obtained through this modified VSS-P&O technique are illustrated in Fig. 15b, d.

The approach used to solve the energy loss problem during the rapid increase of SI is as follows:

1. If  $|\Delta G / \Delta t| < \epsilon$  the VSS-P&O algorithm working;
2. If  $|\Delta G / \Delta t| \geq \epsilon$ ,  $\Delta T = 0$  and  $\Delta R_L = 0$  stop the VSS-P&O technique to work (the switch  $S=0$ ).
  - If  $\Delta G > 0$ ,  $\Delta P > 0$  and  $\Delta V > 0$ , so in this case, inverse the search direction by using the new positive small VSS  $\Delta D_N$ , where  $\Delta D_N = +K \times |\Delta P / \Delta V|$ , where  $K$  is a much smaller scale factor than  $M$  ( $K \ll M$ ).
  - If  $\Delta G > 0$ ,  $\Delta P > 0$  and  $\Delta V < 0$ , so inverse the search direction by using the new negative small VSS  $\Delta D_N$ , where  $\Delta D_N = -K \times |\Delta P / \Delta V|$ .

Through Fig. 16a,c at the rapid decrease in SI, point A jumps to point B near point D (MPPT technique). At point B the VSS-P&O technique receives the information by both parameters  $\Delta P$  and  $\Delta V$  and taking the search

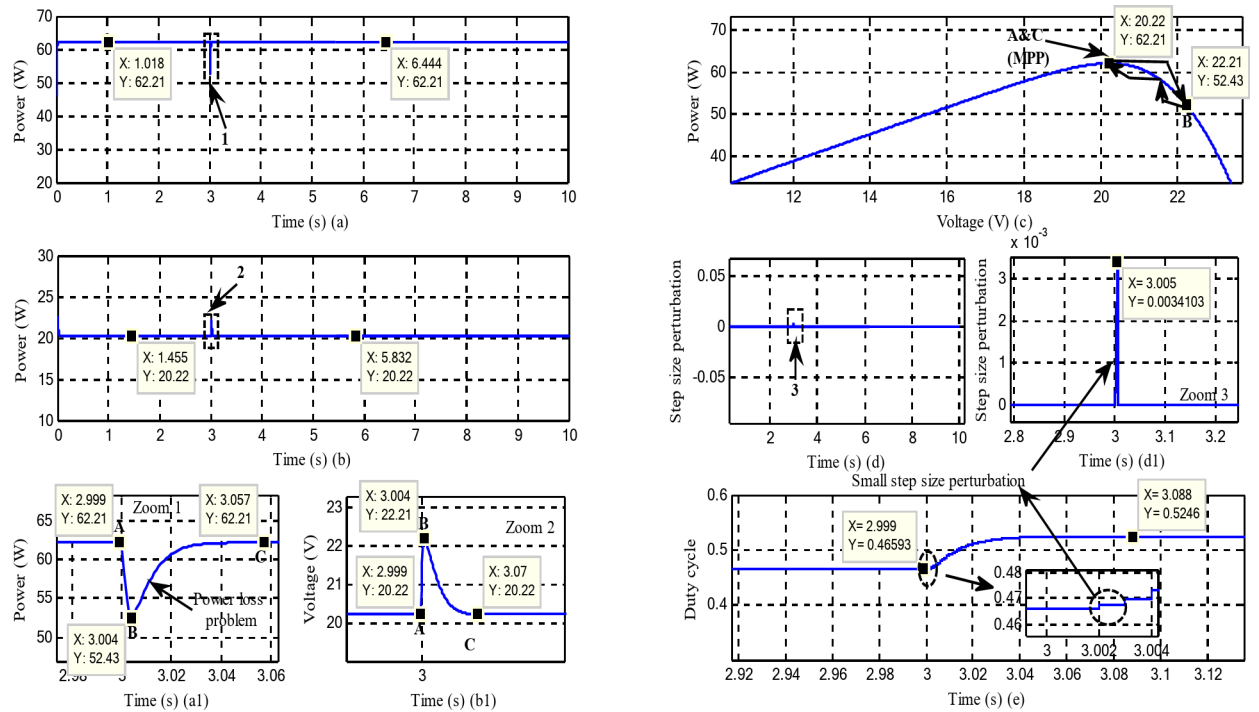


**Fig. 13.** (a) Energy loss problem during increase of resistive load, (b) PV module output voltage in increase of resistive load, (c) PV curve during rapid increase of resistive load, (d) Step size perturbation during rapid increase of resistive load, and (e)  $D$  during rapid increase of resistive load.

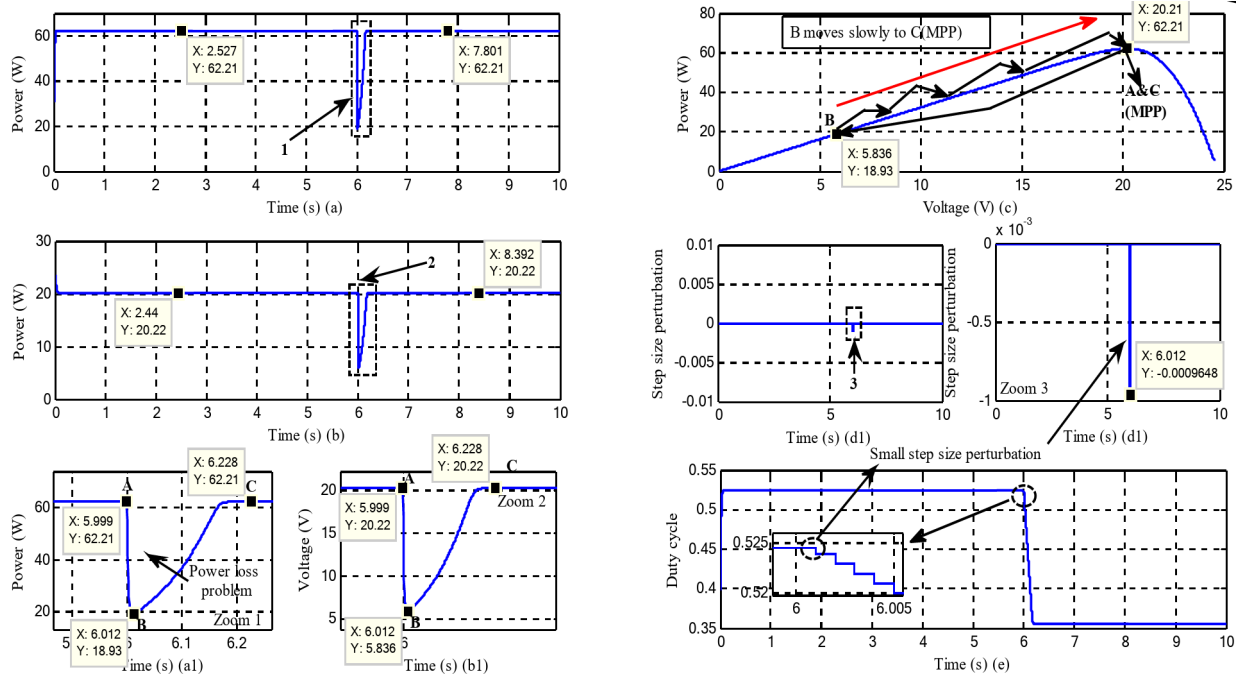


**Fig. 14.** (a) Energy loss problem during decrease of resistive load, (b) PV module output voltage in decrease of resistive load, (c) PV curve during rapid decrease of resistive load, (d) Step size perturbation during rapid decrease of resistive load, and (e)  $D$  during rapid decrease of resistive load.

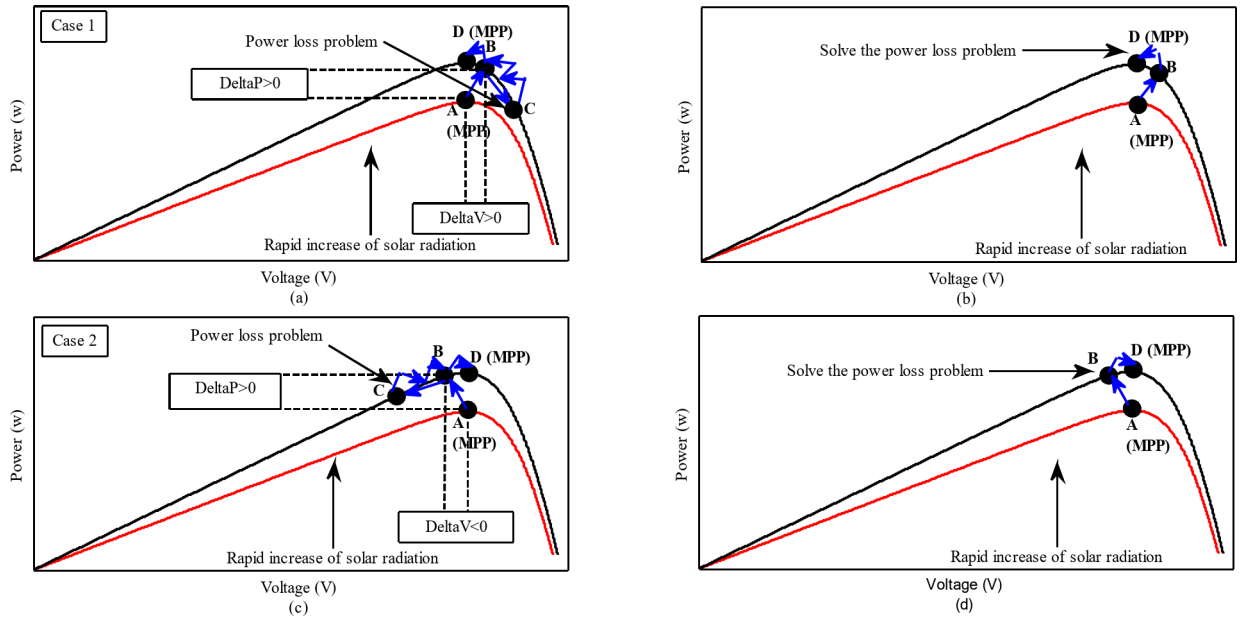


**Fig. 15.** An MPPT approach during rapid increase of solar irradiation: (a) VSS-P&O method in case of positive  $\Delta P$  and  $\Delta V$ , (b) Modified VSS-P&O method in case of positive  $\Delta P$  and  $\Delta V$ , (c) VSS-P&O method in case of positive  $\Delta P$  and Negative  $\Delta V$ , and (d) Modified VSS-P&O method in case of positive  $\Delta P$  and negative  $\Delta V$ .

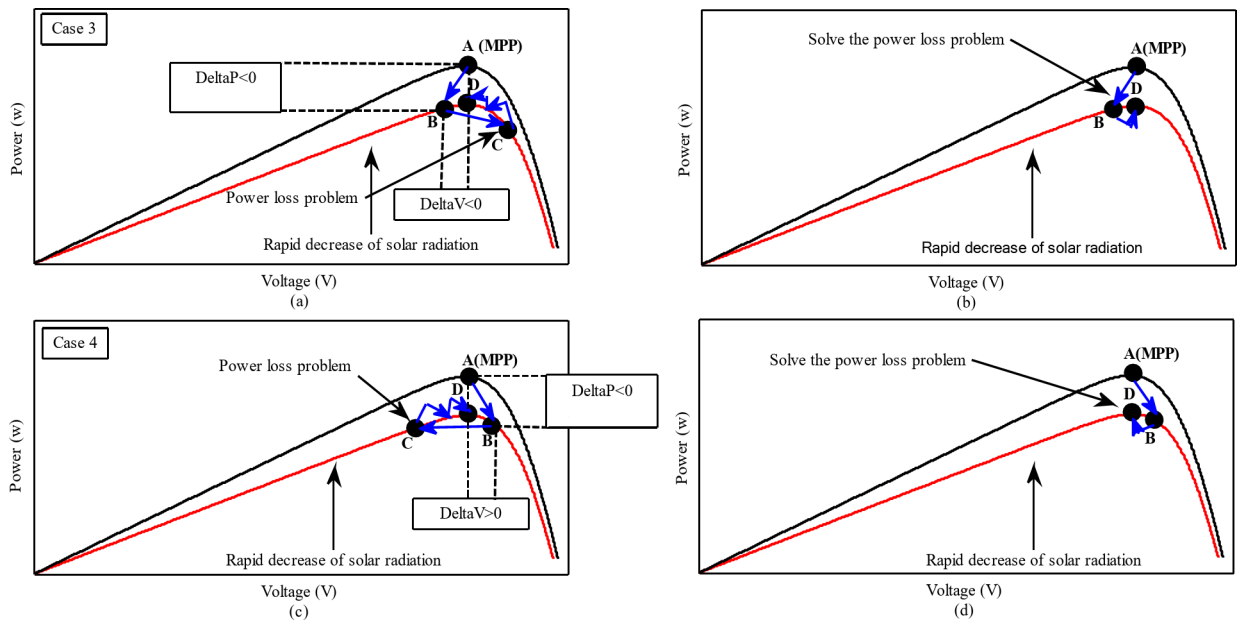


**Fig. 16.** An MPPT Approach during rapid decrease of solar irradiation: (a) VSS-P&O method in case of positive  $\Delta P$  and  $\Delta V$ , (b) Modified VSS-P&O method in case of positive  $\Delta P$  and  $\Delta V$ , (c) VSS-P&O method in case of positive  $\Delta P$  and negative  $\Delta V$ , and (d) Modified VSS-P&O method in case of positive  $\Delta P$  and negative  $\Delta V$ .

direction to find the maximum point D (MPPT technique), but a large step size  $\Delta D_{VSS}$  makes B move to point C far from point D causing the energy loss.

To solve the energy loss problem during the rapid reduce in SI we take the following steps:

1. If  $|\Delta G / \Delta t| < \epsilon$  make the VSS-P&O technique in state on.
2. If  $|\Delta G / \Delta t| \geq \epsilon$ ,  $\Delta T = 0$  &  $\Delta R_L = 0$  stop the VSS-P&O technique to work (the switch  $S = 0$ ), then:

- If  $\Delta G < 0, \Delta P < 0$  and  $\Delta V < 0$  so in this case, the keep the same search direction by using the new negative small VSS perturbation  $\Delta D_N = -K \times |\Delta P / \Delta V|$ .
- If  $\Delta G < 0, \Delta P < 0$  and  $\Delta V > 0$  so in this case, keep the same search direction by using the new positive small VSS perturbation  $\Delta D_N = +K \times |\Delta P / \Delta V|$ .

Figure 16b,d illustrate that after applying the modified approach, we successfully eliminate the issue of power loss.

**Solution method during rapid change of  $T$**

Figure 17 represents the different cases in which energy loss occurs during a rapid increase in decrease in  $T$ . If we want to apply the same previous method that we applied during the rapid change in SI, then the method will succeed only in cases 1 and 2, but in cases 3 and 4 it will fail in one of them because they share the same conditions ( $\Delta T < 0, \Delta P < 0$  and  $\Delta V < 0$ ) as shown in Fig. 17c,d.

To make the modified VSS-P&O technique more efficient, during rapid  $T$  change, we varied its function from a VSS to a small constant step size to avoid decision error.

The Energy loss problem can be solved by using evaluating and changing Eq. (14) to become as follows:

$$\Delta D_{VSS} = \pm M \times \alpha |P(t) - P(t-1)| / |V(t) - V(t-1)| \pm \beta \Delta D_{FSS} \tag{15}$$

where,  $\alpha$  and  $\beta$  are positive real numbers that are either 0 or 1.

Other parameters are used such as  $\Delta T$  (change of  $T$ ) and  $\varepsilon$  to capturing the rapid change of  $T$ .

1. If  $|\Delta T / \Delta t| < \varepsilon$ , in this case the modified VSS-P&O technique make  $S = 1, \alpha = 1$ , and  $\beta = 0$  and working by:  $\Delta D_{VSS} = \pm M \times |P(t) - P(t-1)| / |V(t) - V(t-1)|$ .
2. If  $|\Delta T / \Delta t| \geq \varepsilon, \Delta G = 0$  and  $\Delta R_L = 0$  in this case the modified VSS-P&O technique make  $S = 1, \alpha = 0$  and  $\beta = 1$ , then:
  - a. If  $\Delta P > 0$  and  $\Delta V > 0$  the modified VSS-P&O technique working by:  $\Delta D_{VSS} = -\beta \Delta D_{FSS}$
  - b. If  $\Delta P > 0$  and  $\Delta V < 0$  the modified VSS-P&O technique working by:  $\Delta D_{VSS} = +\beta \Delta D_{FSS}$
  - c. If  $\Delta P < 0$  and  $\Delta V < 0$  the modified VSS-P&O technique working by:  $\Delta D_{VSS} = -\beta \Delta D_{FSS}$

**Solution method during rapid change of resistive load**

Based on the above analysis shown in Figs. 13 and 14, the problem of power loss that occurs during rapid change of resistive load is summarized as shown in Fig. 18.

In the first and second cases at point A, when a rapid change of the resistive load occurs up by a large value, point A moves to the left of point B, far from point MPPT technique, but when the rapid change by a small value, B is near point MPPT technique.

The MPPT-VSS-P&O technique does not allow for good handling under rapidly resistive load changes. In the third and fourth cases, point A moves to the right to point B, further or nearer to the MPPT technique, according to the change in the value of the resistive load (Fig. 19). The VSS-P&O technique fails to capture the MPPT technique in four cases. All cases are related to incorrect step size perturbation during rapid increase or reduction of resistive load with big and small values.

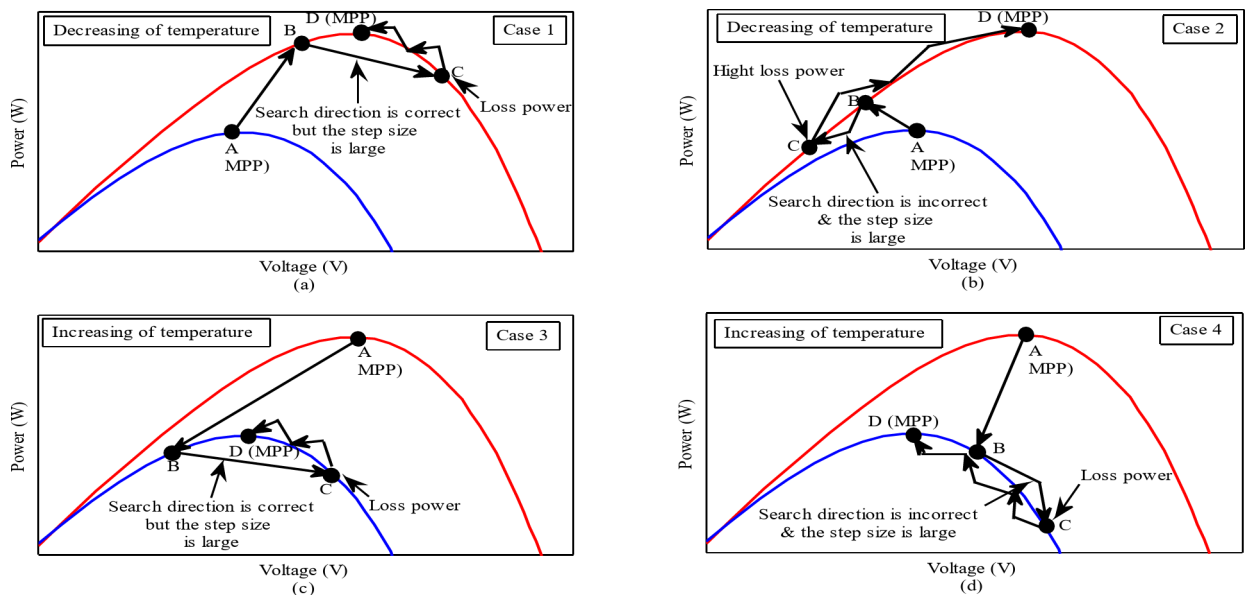


**Fig. 17.** Energy loss problem of the VSS-P&O during PV module exposed to (a), (b) decreasing  $T$ , (c) and (d) increasing  $T$ .

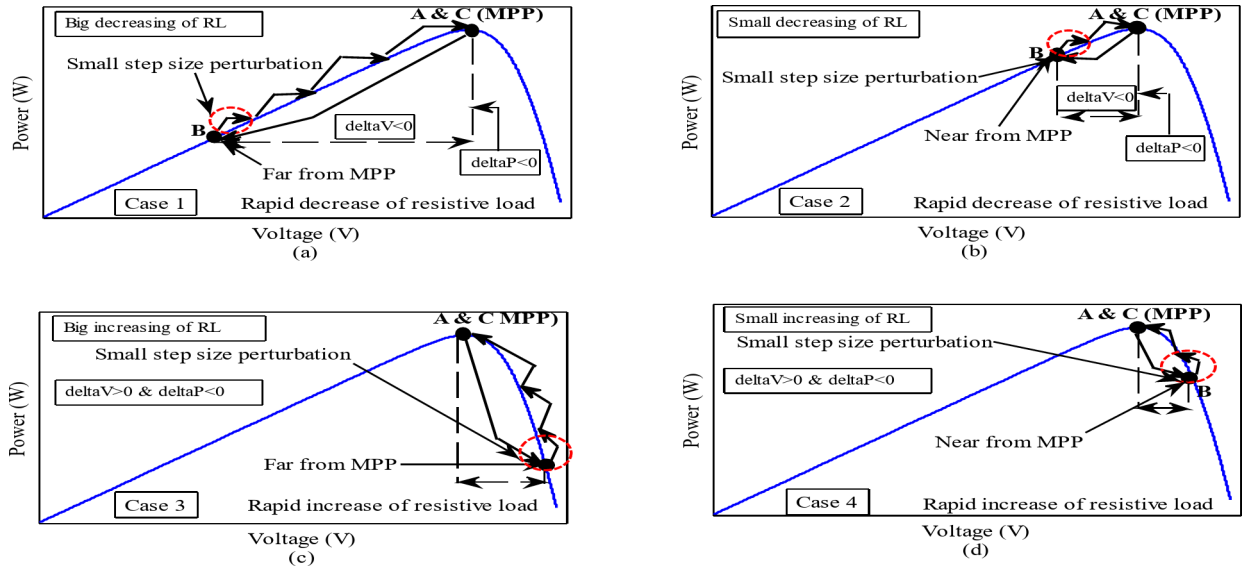


**Fig. 18.** Energy loss problem of the VSS-P&O during PV module connected to (a) Big decreasing of resistive load, (b) Small decreasing of resistive load, (c) Big increasing of resistive load, and (d) small increasing of resistive.

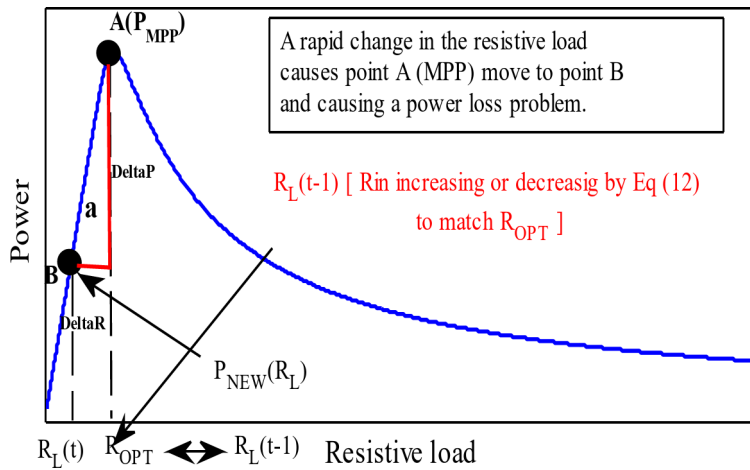


**Fig. 19.** Power-resistive load characteristic.

As shown in Figs. 13 and 14, when a rapid change in the resistive load, the wrong decision in the small value of the step size perturbation given by the VSS-P&O technique causes slowly speed to reach the optimal  $D (D_{opt})$  that corresponds to the MPPT technique, thus causing a loss energy problem.

To minimize power loss, the step size perturbation should be increased rather than decreased during rapid changes in the resistive load. This ensures a faster convergence to the MPPT technique (Point C).

To solve the loss of power which is the main problem investigated in this research and as a contribution; a new calculation of the VSS based on the MPPT-VSS-P&O technique has been developed. It can be noted that the designed technique is described by the simplicity of modeling. The designed P&O-VSS technique process is expressed by:

$$\Delta D_L = \lambda \pm \left| \frac{\Delta R_L \times \Delta P}{2} \right| \tag{16}$$

So the  $D$  during the rapid change of resistive load is:

$$D(t) = D(t-1) \pm \lambda \times \left| \frac{\Delta R_L \times \Delta P}{2} \right| \tag{17}$$

where,  $D(t)$  and  $D(t-1)$  are the present and previous  $D$  respectively.

$\Delta P$ : Change in power is determined as the difference between the new (at point B) and old values (at point A);

$\Delta R_L$ : Change in resistive load is determined as the difference between the new (at point B) and old values (at point A).

$\lambda$ : Scale factor used to fine-tune the step-size perturbation at the design stage.

This idea is based on the use of the theory of shapes (triangle), which is a basic relationship in geometry. The formula for the area of a triangle is half the product of its base and height, where the height represents the change in power [ $P(t)-P(t-1)$ ] and the base represents the change in the resistive load [ $(R_L(t)-R_L(t-1))$ ].

$$\Delta R_L = R_L(t) - R_L(t-1) \quad (18)$$

$$\Delta R_L = \frac{V_L(t)}{I_L(t)} - \frac{V_L(t-1)}{I_L(t-1)} \quad (19)$$

Based on this idea, a better estimate can be given for the step size by using the Eq. (17). Thus the length of the  $D$  controls becomes very dynamic and fast during the rapid changes in resistive load.

During rapid change of resistive load, the modified VSS-P&O technique captures the change by  $|\Delta R_L / \Delta t| > \varepsilon$ .

To solve the energy loss problem at the rapid change of resistive load we take the following steps:

1. If  $|\Delta R_L / \Delta t| < \varepsilon$ , the VSS-P&O technique is state on ( $S = 1$ ,  $\alpha = 1$  &  $\beta = 0$ ).
2. If  $|\Delta R_L / \Delta t| \geq \varepsilon$ ,  $\Delta G = 0$  and  $\Delta T = 0$  stop the VSS-P&O to work (the switch  $S = 0$ ), then:
  - If  $\Delta V < 0$  and  $\Delta P < 0$ , the VSS-P&O technique is “off” and the  $D$  decreasing automatically by  $\Delta D_L$ .
3. If  $\Delta V > 0$  &  $\Delta P < 0$ , the VSS-P&O technique is “off” and the  $D$  increasing automatically by  $\Delta D_L$ .

### Simulation analysis

In this section, the modified VSS-P&O approach is implemented using MATLAB, where the effectiveness and efficiency of this strategy in improving the properties of the studied system are verified. This proposed strategy is shown in Fig. 20. Table 2 represents the system parameters used in this study. Several different tests are proposed to study the performance and behavior of this proposed approach.

#### Test under variation in SI with constant $T$ (25 °C)

To verify the tracking competence of the modified VSS-P&O technique, the approach of Fig. 20 is realized in MATLAB. Figure 21 represents the simulation results of this realization. The VSS-P&O, FL-P&O control, old P&O technique, and modified VSS-P&O technique were simulated in the same different rapid change conditions as shown in Fig. 21b. Figure 21a shows the comparison between the powers delivered by the VSS-P&O strategy, FL control, old P&O technique, and modified VSS-P&O technique and the derivative curve of SI and the  $D$ . It can be seen from these figures that the modified algorithm has succeeded in a large extent in capturing the rapid change of SI as shown in Fig. 21c. The energy loss problem is solved by deactivating the VSS-P&O technique and activating the modified VSS-P&O strategy by reversing the step size perturbation in the rapid increase of SI by making it positive and small to do the research for the MPPT technique in the correct direction as shown in Fig. 21d1 and keeping the same direction research of (MPPT) when the rapid decrease of SI exist by using a negative small step size perturbation as shown in Fig. 21d2.

Figure 21 shows the behavior of the PV system to ward off different rapid changes in SI for the four approaches.

In Fig. 22, it can be seen that VSS-P&O, FL control, and old P&O approaches show a power loss problem when there is a rapid change in SI, whereas it is this problem of energy loss does not exist in the case of the modified VSS-P&O technique.

#### Test under variation in $T$ with constant SI (1000 W/m<sup>2</sup>)

Figure 23 represents the simulation results of the PV panel connected directly to a variable resistive load without the presence of the DC-DC converter under a constant of SI ( $G = 1000 \text{ W/m}^2$ ) and different values of  $T$ : 35 °C, 40 °C, 45 °C, 46.80 °C, 48 °C and finally 50 °C.

Figure 23 shows that for each  $T$  there is a PV characteristic curve that differs from the PV characteristic curve for another  $T$  value and thus a different MPPT approach for any  $T$  change as well shown in Fig. 23b.

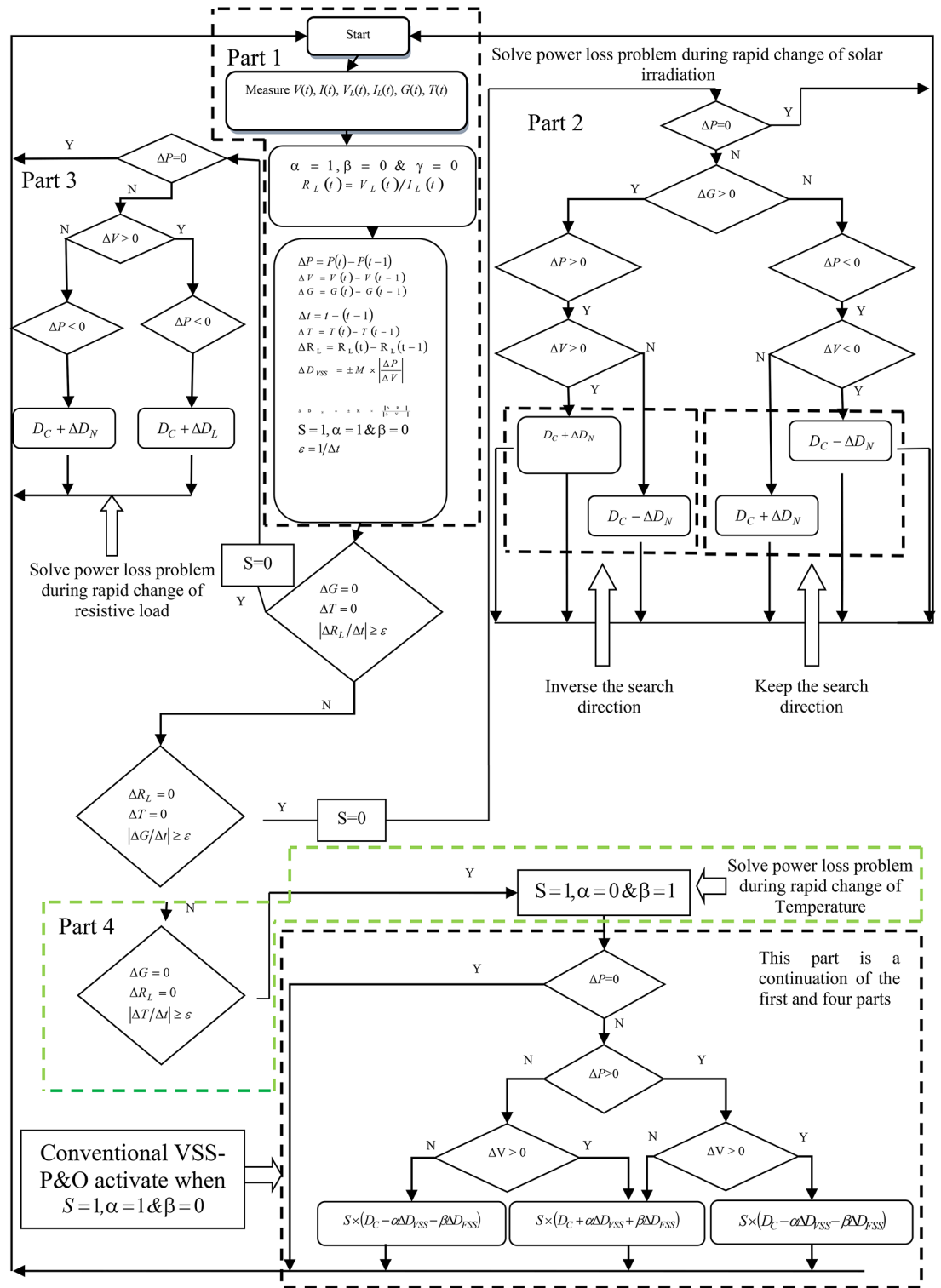
The output PV power of the VSS-P&O strategy, FL control, old P&O technique, and modified VSS-P&O approaches when the  $T$  varies rapidly are shown in Fig. 24. In each case, the SI is rested as  $1000 \text{ W/m}^2$ , and the  $T$  is rapidly increasing from 35 to 40 °C at 2 s, from 40 to 45 °C at 3 s, from 45 to 50 °C at 5 s, and rapidly reduce from 50 to 48 °C at 6 s and finally increase from 48 °C to 46.8 °C at 7 s.

Figure 24 shows the modified VSS-P&O technique succeeded in tracking the MPP with zero oscillations and avoiding the problem of energy loss compared with the other three approaches under the rapid changes in  $T$ .

### Explanation of the proposed algorithmic steps

The algorithm for this designed approach is divided into four main parts, with each part playing a vital role in achieving the algorithm's ultimate goal.

Part 1. Variable definition and condition specification: This part is the most critical, as it involves defining the variables necessary for the algorithm and specifying the conditions and criteria required to achieve the



**Fig. 20.** Modified VSS-MPPT-P&O approach.

desired goal. This part focuses on capturing the MPP and addressing oscillation issues, thereby improving the algorithm’s competence and ensuring its stability.

**Part 2.** Analysis of rapid changes in SI: In this part, essential information about rapid changes in SI is gathered and analyzed accurately, with the application of the  $D$  illustrated in Fig. 20-Part 2.

**Part 3.** Analysis of rapid changes in load resistance: This part focuses on exploring rapid changes in load resistance and analyzing available data, applying the appropriate  $D$  as depicted in Fig. 20-Part 3.

Photovoltaic parameters	
Parameter	Value
$I_{SC}$ (Short circuit current at standard conditions)	3.25 A
$R_s$ (Series-Resistance)	0.015 Ohm
$A$ (Diode ideality factor)	1.2
$I_0$ (saturation current)	$8.225 \times 10^{-12}$ A
$q$ (Electron charge)	$1.6 \times 10^{-19}$ C
$K$ (Boltzmann constant)	$1.38 \times 10^{-23}$ J/K
$T_{SC}$ (Temperature at standard conditions)	25 °C
$V_{OC}$ (Open-Circuit Voltage)	24.8 V
$R_{sh}$ (Parallel-Resistance)	30 Ohm
$G$ (Solar irradiation at standard Conditions)	1000 W/m <sup>2</sup>
$N_s$ (Number of solar cells in series)/panel	36
$N_p$ (Number of solar cells in parallel)/panel	1

**Table 2.** Simulation parameters.

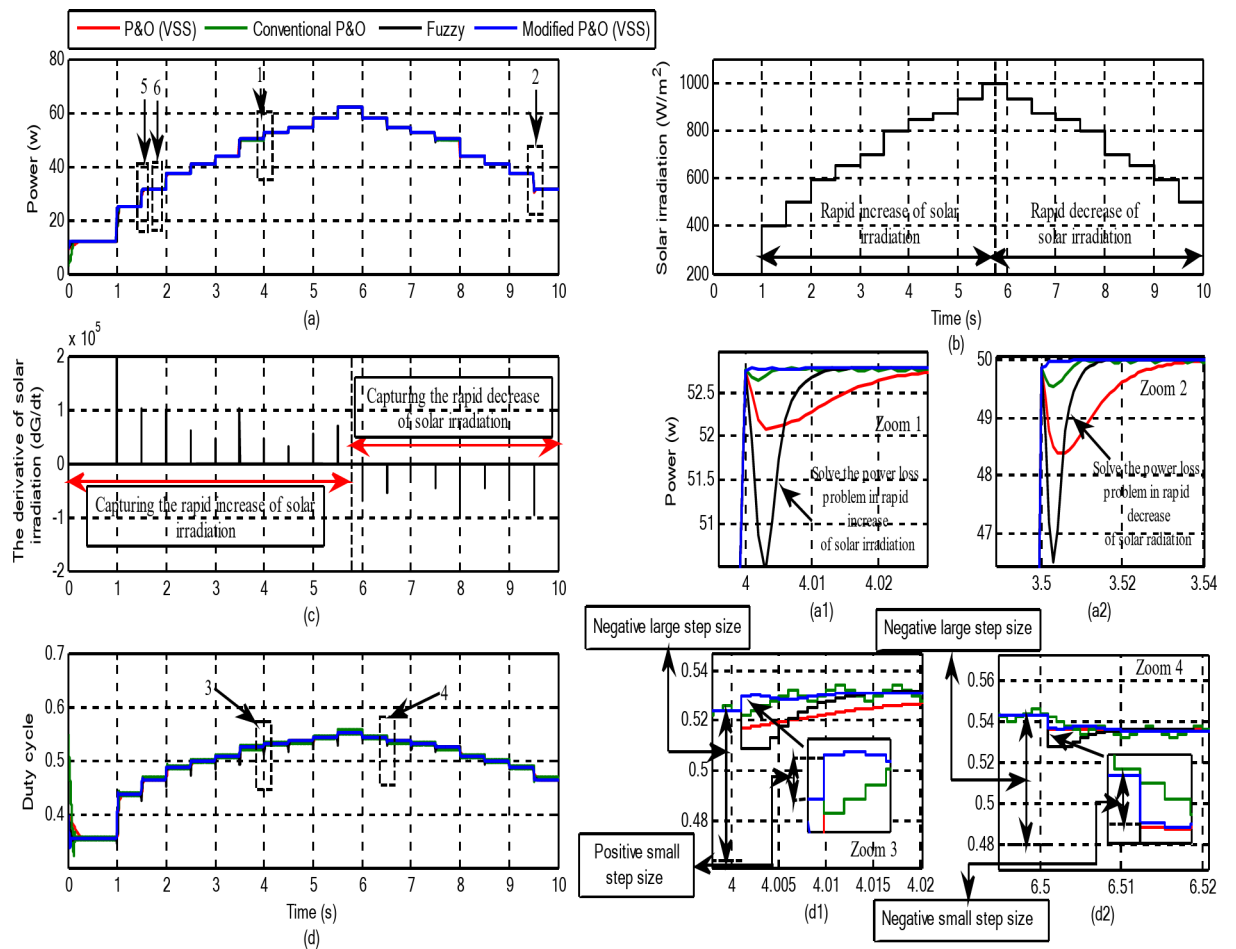


**Fig. 21.** (a) Comparison of PV power under variation in SI, (b) SI levels, (c) dG/dt curve, and (d) D.

Part 4. Analysis of rapid  $T$  changes: In this final part, rapid  $T$  changes are explored, and available data is analyzed, with the application of the suitable  $D$  as depicted in Fig. 20 (Part 4).

In summary, the algorithm involves the process of defining variables and required conditions, analyzing rapid changes in SI, load resistance, and  $T$ , and applying appropriate duty cycles to ensure stability and effective system competence.

The steps of the algorithm can be summarized in Table 3.

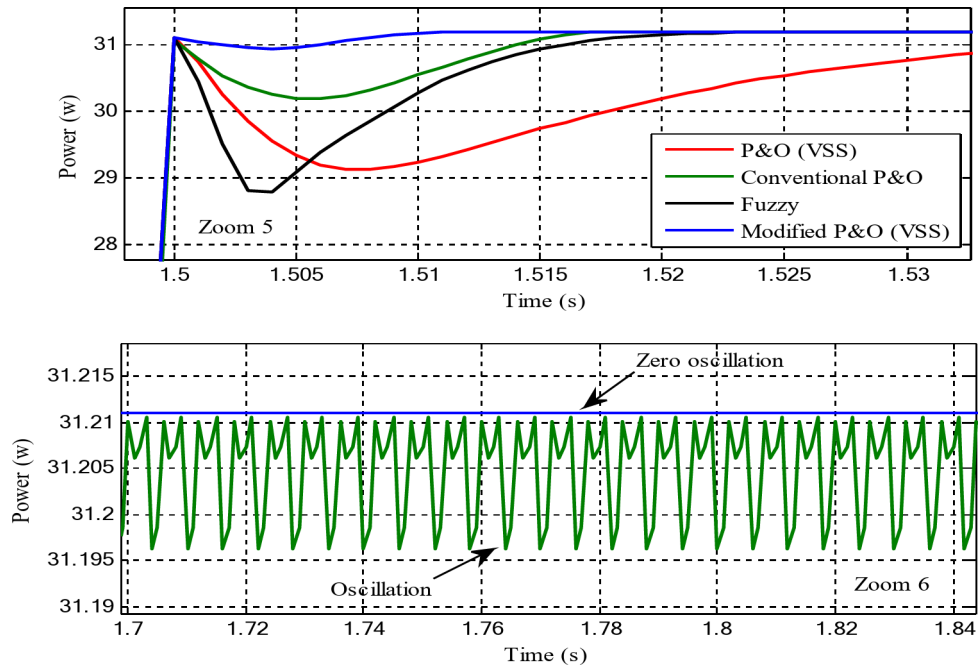


**Fig. 22.** Zoom of power under variation in SI with  $T = 25\text{ }^{\circ}\text{C}$ .

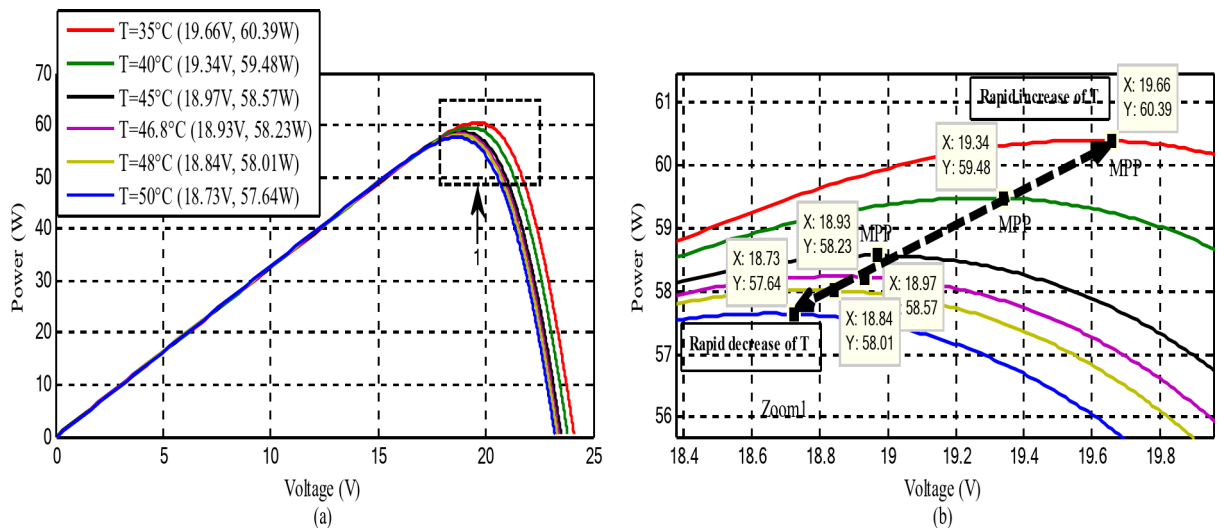


**Fig. 23.** (a) Different levels of  $T$  with  $G = 1000\text{ W/m}^2$  and (b) Enlarged view showing variations in  $T$  levels.

Figures 21d1, d2, 25c1, c2 illustrate the transient response of the buck-boost converter when subjected to rapid changes in irradiance. The proposed control method significantly reduces overshoot and oscillations compared to conventional VSS-P&O approaches, leading to improved voltage stability and minimized power losses.

**Test under variation in load resistance with constant SI ( $G = 1000\text{ W/m}^2$ ) and  $T (25\text{ }^{\circ}\text{C})$**

The PV panel is connected to a variable resistive load through a DC-DC converter with the MPPT strategy. The VSS-P&O technique, FL control, old P&O technique, and modified VSS-P&O approaches are used to make a comparison of their solve the energy loss problem, and the tracking ability. The tracking ability is studied in terms of the energy loss problem, the steady-state oscillation, and the speed of RT during a constant and rapid reduction and increase of the resistive load.

During the period of resistive load ( $R = 5\text{ }\Omega$ ) shown in Fig. 25, the modified VSS-P&O-MPPT technique reduces the  $D$  to ( $D = 0.465$ ) and increases the input resistance  $R_{in}$  by using Eq. (12) to match ( $R_{opt} = 6.552\text{ }\Omega$ ).

The energy oscillation of the operating point around the MPPT technique using a modified VSS-P&O strategy is zero oscillations than that of the old P&O technique.

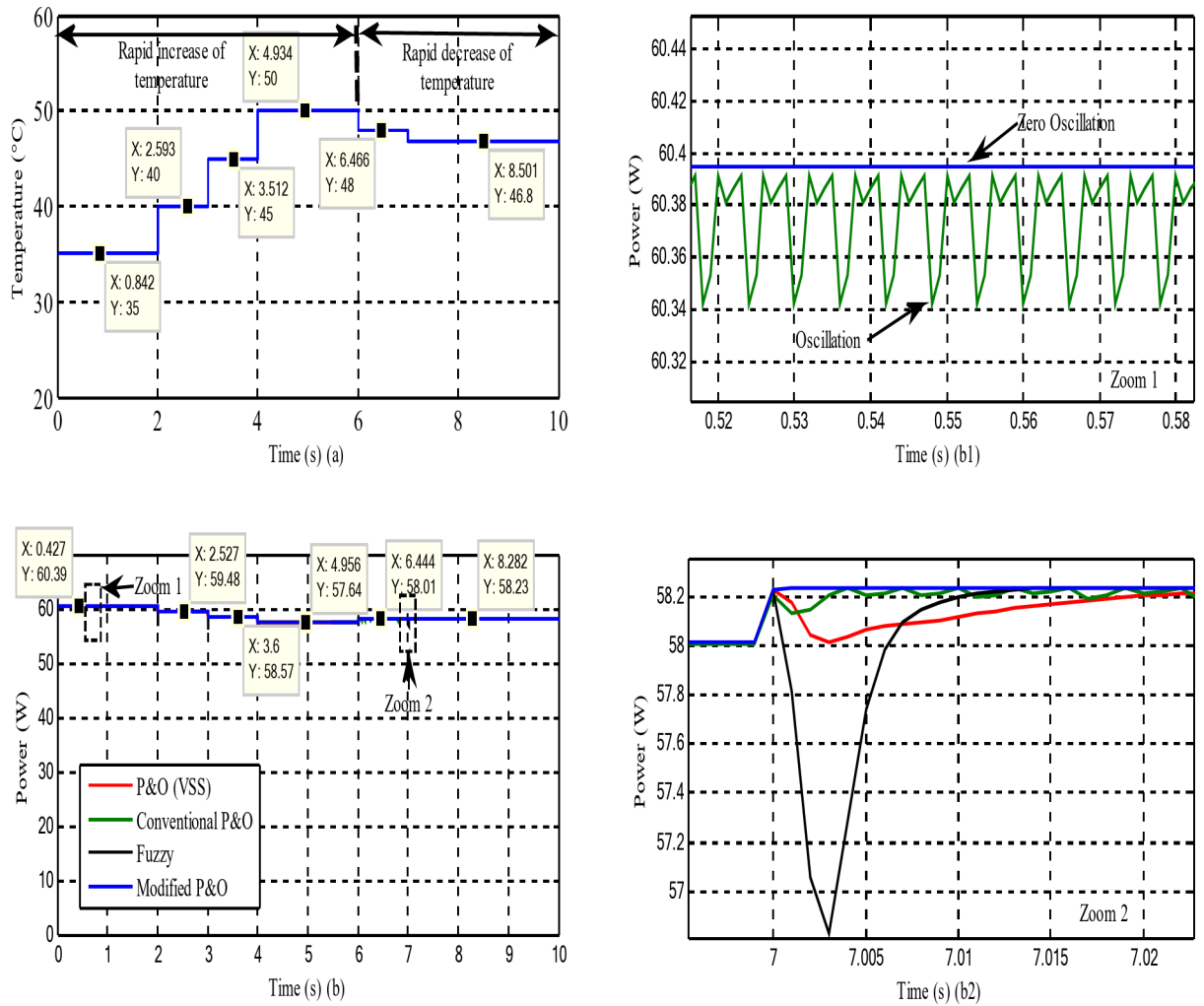


**Fig. 24.** (a)  $T$  levels and (b) Comparison of PV power under variation in  $T$ .

Step	Description	Condition	Active parts	Objectives
1. Variable definition and condition specification	Defining the variables necessary for the algorithm and specifying the conditions and criteria required to achieve the desired goal	$\Delta G = 0, \Delta T = 0, \Delta R_L = 0$	Part 1	Achieve the MPP without perturbations
2. Analysis of rapid changes in SI	Gathering information about rapid changes in SI and analyzing it accurately	$\Delta R_L = 0, \Delta T = 0,  \Delta G / \Delta t  \geq \epsilon$	Part 1 + Part 2	Eliminate the energy loss
3. Analysis of rapid changes in load resistance	Exploring rapid changes in resistive load and analyzing the available data	$\Delta G = 0, \Delta T = 0,  \Delta R_L / \Delta t  \geq \epsilon$	Part 1 + Part 3	Eliminate the energy loss
4. Analysis of rapid changes in $T$	Exploring rapid changes in temperature and analyzing the available data	$\Delta G = 0, \Delta R_L = 0,  \Delta T / \Delta t  \geq \epsilon$	Part 1 + Part 4	Eliminate the energy loss

**Table 3.** Steps of the designed approach.

Figure 25a1, a2 show that the modified control was able to solve the problem of energy loss during the rapid change of the resistive load. When the resistive load is rapidly increased from  $5 \Omega$  to  $8 \Omega$  as shown in Fig. 25a,  $R_{in}$  increases rapidly from  $6.522 \Omega$  to  $8 \Omega$  at point B, shown in Fig. 25a1. At this moment, the designed MPPT technique tries to maintain the operating point of the PV panel by moving point B to point C rapidly by using Eq. (17) to reduce the energy loss problem compared with other MPPT approaches, especially the VSS-P&O technique and FL control which did not well estimate the step size perturbation during the rapid change of the resistive load which makes it use small step size perturbation (decision error) and make point B move to operating point C by a slow speed as shown in Fig. 25c1 and this is what causes the energy loss problem as shown in Fig. 25a1.

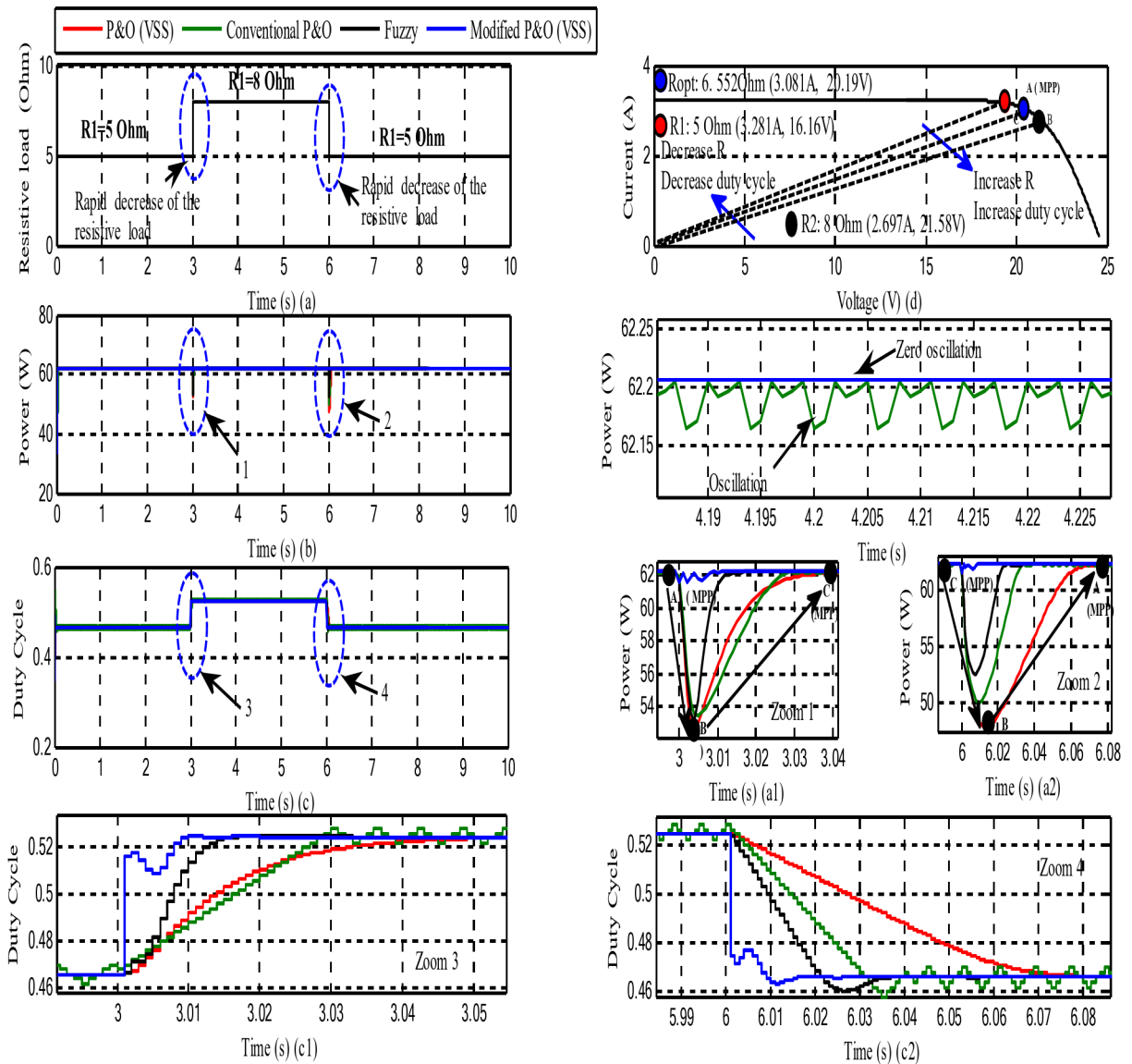


**Fig. 25.** (a) Variations in resistive load, (b) Comparison of PV power under variation in resistive load, (c)  $D$ , and (d) Current–voltage features and optimal input resistances of the PV panel.

The designed MPPT technique increases the  $D$  from ( $D=0.464$ ) to ( $D_{opt}=0.525$ ) in a time equal to (3.01 s), while the other approaches were as follows: VSS-P&O (3.09 s), FL control (3.018 s) and old P&O technique (3.028 s) as shown in Fig. 25c1.

The same approach applies when the resistive load is rapidly decreased from  $R_{in}$  to  $5 \Omega$ . From Fig. 25, it is noted that the modified VSS-P&O technique gives satisfactory results compared to the other approaches (as shown in Fig. 25a) when a rapid change in the resistive load occurs.

In Table 4, the numerical results for the various approaches used in this work are given for the MPPT technique. From this table, it is noted that the modified P&O-VSS strategy provided better results for efficiency compared to the P&O technique, P&O-VSS, and FL controls. Therefore, the Efficiency value was 99.90%, 99.95%, 99.94%, and 99.98% for conventional P&O strategy, P&O-VSS strategy, FL control, and modified P&O-VSS technique, respectively (In the case of rapid change in SI). In terms of RT, it is noted that the modified P&O-VSS technique provided a much better time than the P&O technique, P&O-VSS strategy, and FL control, which is a positive thing and indicates that the designed approach has a very fast DR. The time values were 0.109 s, 0.213 s, 0.08 s, and 0.032 s for the P&O technique, P&O-VSS approach, FL control, and modified P&O-VSS strategy, respectively (In the case of rapid change in SI). The energy loss (Drift) value for the approaches was 0.11 W, 0.66 W, 2.27 W, and 0 W for the P&O approach, P&O-VSS approach, FL control, and modified P&O-VSS strategy, respectively (In the case of rapid change in SI). Therefore, the designed approach provided an excellent value for energy loss compared to other approaches, which indicates its efficiency and high competence.

In the case of rapid  $T$  change, the designed approach provided excellent results in terms of efficiency (%), power loss (drift), and RT (s) compared to the rest of the approaches, and this is proven by the numerical results

MPPT approaches	Rapid change in SI			Rapid change in T			Rapid change in resistive load		
	Efficiency (%)	Energy loss (Drift) W	RT (s)	Efficiency (%)	Energy loss (Drift) W	RT (s)	Efficiency (%)	Energy loss (Drift) W	RT (s)
P&O	99.90%	0.11	0.109	99.91%	0.05	0.007	99.95%	12.22	0.034
P&O-VSS	99.95%	0.66	0.213	99.97%	0.61	0.027	99.97%	14.4	0.032
FL control	99.94%	2.27	0.08	99.98%	2.4	0.004	99.97%	9.84	0.01
Modified P&O-VSS	99.98%	0	0.032	99.99%	0.04	0.003	99.98%	0.28	0.004

**Table 4.** Quantitative comparison of MPPT methods.

References	MPPT technique	Efficiency	Sensors	Steady-state oscillation
64	Incremental conductance	High	Voltage and current	Yes
65	Neural network	High	User knowledge	
	Short circuit current	Low	Current	
	Open circuit voltage	Low	Voltage	
	Short circuit current		Current	
	P&O (variable perturbation size)	High	Current and voltage	No
P&O (fixed perturbation size)	Low	Yes		
66	PSO	High		No
67	Combining fractional-order and FLC			Yes
68	Fast converging approach			
69	Differential evolution-based MPPT			
70	Modified incremental conductance			
Designed MPPT approach			Voltage, irradiation, and energy	No

**Table 5.** Comparison between different papers and designed approach.

listed in Table 4. So, this designed approach performed well. Distinctive, making it one of the most important solutions that can be relied upon in the future. Also, it is noted that the modified P&O-VSS approach provided numerical results in the case of rapid change in resistive load in terms of efficiency (%), power loss (drift), and RT (s) compared to other approaches, which is positive.

In Table 5, a comparison with other works is made. In this table, the completed work is compared with other work in terms of the type of MPPT approach used, and efficiency sensors' steady-state oscillation. Accordingly, the completed work has similarities and differences with other works, where among the differences lies in the type of MPPT approach used in control. Also, the suggested approach has a distinctive competence in terms of steady-state oscillation compared to some scientific papers, which is a positive thing that indicates the superiority of the designed approach, making it a suitable solution in the future. Also, in terms of Efficiency, the designed approach has high competence compared to some research works, which is a good thing that proves the superiority of the designed approach.

## Conclusions

This study introduced an innovative approach to enhance the performance of PV systems by designing and optimizing an MPPT technique using a VSS-P&O algorithm. The achieved results demonstrated the superiority of the proposed method over traditional techniques in terms of efficiency, rapid response, reduced oscillations, and minimized energy loss. The system achieved an efficiency of 99.98% while nearly eliminating energy loss during rapid changes in SI, temperature, and resistive load. The improved algorithm stood out for its simplicity and low cost, making it a practical and sustainable solution for SE systems. Based on these promising findings, future research could focus on enhancing the algorithm to address partial shading conditions, experimentally validating its performance in real-world scenarios, integrating it into hybrid systems that combine multiple energy sources, and leveraging artificial intelligence to improve its response to environmental changes. The proposed method marks a significant step toward achieving energy sustainability and reducing reliance on non-renewable energy sources.

## Data availability

Data available on request from the authors. The datasets used and/or analysed during the current study available from the corresponding author on reasonable request. In the event of communication, the first author (Habib Benbouhenni, E-mail: habib.benbouhenni@enp-oran.dz) will respond to any inquiry or request.

Received: 28 January 2025; Accepted: 20 March 2025

Published online: 05 April 2025

## References

- Moez, A., Sahbi, A., Habib, B. Z. & Mohamed, C. A novel fuzzy control strategy for maximum power point tracking of wind energy conversion system. *Int. J. Smart Grid-ijSmartGrid*. **3** (3), 120–127. <https://doi.org/10.20508/ijsmartgrid.v3i3.63.g58> (2019).
- Ahmed, S. A., Lamki, A., Abdulhakim, H., Hussein, A. K. & A. & Techno economic design and analysis of a hybrid renewable energy system for Jazirat al Halaniyat in Oman. *Int. J. Renew. Energy Res. IJRES*. **13** (3), 1039–1050. <https://doi.org/10.20508/ijrer.v13i3.13679.g8778> (2024).
- Willian, M. F., de Souza Reis, R. & Lucas, G. Remote monitoring and analysis of productivity indicators of photovoltaic energy generation systems. *Int. J. Smart Grid-ijSmartGrid*. **8** (1), 20–26. <https://doi.org/10.20508/ijsmartgrid.v8i1.322.g332> (2024).
- Elmer, R. A. L. Wind energy potential by the Weibull distribution at High-Altitude Peruvian highlands. *Int. J. Smart Grid-ijSmartGrid*. **5** (3), 113–120. <https://doi.org/10.20508/ijsmartgrid.v5i3.199.g154> (2021).
- Zheng, C. W. et al. CMIP5-Based wave energy projection: Case studies of the South China sea and the East China sea. *IEEE Access*. **7**, 82753–82763. <https://doi.org/10.1109/ACCESS.2019.2924197> (2019).
- Djabeur Mohamed, S. Z. et al. Optimized controller design for renewable energy systems by using deep reinforcement learning technique. *Int. J. Renew. Energy Res. IJRES*. **14** (1), 101–110. <https://doi.org/10.20508/ijrer.v14i1.14362.g8854> (2024).
- Syed, Z. R. H., Junaid, A. M., Minhaj, A. M. & Asad, O. Remote real-time power analysis and management system. *Int. J. Smart Grid-ijSmartGrid*. **5** (3), 128–137. <https://doi.org/10.20508/ijsmartgrid.v5i3.212.g156> (2023).
- Mohammed, F., Ahmed, E., Mohamed, N. & Tamou, N. Control and optimization of a wind energy conversion system based on Doubly-Fed induction generator using nonlinear control strategies. *Int. J. Renew. Energy Res.-IJRES*. **9** (1), 44–45. <https://doi.org/10.20508/ijrer.v9i1.8812.g7619> (2019).
- Srikanth, G. B. & Loveswara, R. B. Power quality improvement in hybrid renewable energy source grid-connected system with grey Wolf optimization. *Int. J. Renew. Energy Res.-IJRES*. **10** (3), 1071–1082. <https://doi.org/10.20508/ijrer.v10i3.11318.g8004> (2020).
- Dharamalla, C. S., Rama, R. P. V. V. & Kiranmayi, R. Improvement of power quality in grid integrated smart grid using fractional-order fuzzy logic controller. *Int. J. Renew. Energy Res.-IJRES*. **12** (2), 960–969. <https://doi.org/10.20508/ijrer.v12i2.12948.g8483> (2022).
- Savarapu, C. S., Muthamizhan, T., Mohammad, A. & Chandra, S. D. Wavelet-ANN based detection of fault location of hybrid renewable energy sources connected power transmission system. *Int. J. Renew. Energy Res.-IJRES*. **14** (3), 551–562. <https://doi.org/10.20508/ijrer.v14i3.14396.g8921> (2024).
- Amira, E., Amr, I., Abdellatif, A. & Shaaban, S. Aerodynamic performance and structural design of 5 MW multi rotor system (MRS) wind turbines. *Int. J. Renew. Energy Res.-IJRES*. **12** (3), 1495–1505. <https://doi.org/10.20508/ijrer.v12i3.13343.g8535> (2022).
- Ercan, E., Selim, S. & Fevzi, C. B. Analysis model of a small scale counter-rotating dual rotor wind turbine with double rotational generator armature. *Int. J. Renew. Energy Res.-IJRES*. **8** (4), 1849–1858. <https://doi.org/10.20508/ijrer.v8i4.8235.g7549> (2018).
- Sara, K., Khoukha, I., El Madjid, B., Habib, B. & Emad, A. A direct vector control based on modified SMC theory to control the double-powered induction generator-based variable-speed contra-rotating wind turbine systems. *Energy Rep.* **8**, 15057–15066. <https://doi.org/10.1016/j.egy.2022.11.052> (2022).
- Hong, V. P. N., Van, T. N. & Van, H. N. A combined strategy to improve operational efficiency of microgrids with high integration of solar and wind energy. *Int. J. Renew. Energy Res. IJRES*. **13** (3), 1247–1258. <https://doi.org/10.20508/ijrer.v13i3.14194.g8797> (2024).
- Saad, A. M. A. et al. Technical evaluation of a superconducting fault current limiter for a microgrid with Wind-PV hybrid generation. *Int. J. Renew. Energy Res.-IJRES*. **14** (3), 538–550. <https://doi.org/10.20508/ijrer.v14i3.14740.g8920> (2024).
- Sahar, A. N. et al. Optimal power management and control of hybrid photovoltaic-battery for grid-connected doubly-fed induction generator based wind energy conversion system. *Int. J. Renew. Energy Res.-IJRES*. **12** (1), 408–421. <https://doi.org/10.20508/ijrer.v12i1.12770.g8422> (2022).
- Aysar, M. Y. Energy management of a stand-alone DC microgrid based on PV/wind/battery/ diesel gen. Combined with supercapacitor. *Int. J. Renew. Energy Res.-IJRES*. **9** (4), 1811–1826. <https://doi.org/10.20508/ijrer.v9i4.10094.g7784> (2019).
- Hassan, A. Impact of on-Load tap changers and smart controllers on the distributed renewable energy hosting capacity. *Int. J. Smart Grid-ijSmartGrid*. **6** (4), 132–135. <https://doi.org/10.20508/ijsmartgrid.v6i4.261.g249> (2022).
- Meryeme, A., Mohammed, O. & Mohamed, M. An optimal energy management of grid-connected residential photovoltaic-wind-battery system under step-rate and time-of-use tariffs. *Int. J. Renew. Energy Res.-IJRES*. **10** (4), 1829–1843. <https://doi.org/10.20508/ijrer.v10i4.11448.g8093> (2022).
- Khelifi, B., Ben Salem, F., Ali, Z. M., Hsan, H. A. A. & Stand-Alone PV-PEMFC system based SM-ANN-MPPT controller: Solar pumping application using PMSM. *Int. J. Renew. Energy Res.-IJRES*. **11** (2), 662–672. <https://doi.org/10.20508/ijrer.v11i2.11977.g8188> (2021).
- Elbarbary, Z. M. S., Cheema, K. M., Al-Gahtani, S. F. & El-Sehiemy, R. A. High gain chopper supplied from PV system to fed synchronous reluctance motor drive for pumping water application. *Sci. Rep.* **12**, 15519. <https://doi.org/10.1038/s41598-022-19671-x> (2022).
- Elbarbary, Z. M. S. & Alranini, M. A. Review of maximum power point tracking algorithms of PV system. *Front. Eng. Built Environ.* **1** (1), 68–80. <https://doi.org/10.1108/FEBE-03-2021-0019> (2021).
- Khalid, Y., Samaa, A., Mahmoud, A., Adel, E. M. Y. & Rebha, D. S. Machine learning techniques for solar power output predicting. *Mach. Learn. Tech. Solar Power Output Predicting* **8** (2), 98–107. <https://doi.org/10.20508/ijsmartgrid.v8i2.341.g356> (2024).
- Alaas, Z., Elbarbary, Z. M. S. & Rezvani, A. Analysis and enhancement of MPPT technique to increase accuracy and speed in photovoltaic systems under different conditions. *Optik* **289**, 171208. <https://doi.org/10.1016/j.ijleo.2023.171208> (2023).
- Ibrahim, N. F. et al. Operation of grid-connected PV system with ANN-based MPPT and an optimized LCL filter using GRG algorithm for enhanced power quality. *IEEE Access*. **11**, 106859–106876. <https://doi.org/10.1109/ACCESS.2023.3317980> (2023).
- Liu, H. D., Lin, C. H., Pai, K. J. & Lin, Y. L. A novel photovoltaic system control strategies for improving hill climbing algorithm efficiencies in consideration of radian and load effect. *Energy. Conv. Manag.* **165**, 815–826. <https://doi.org/10.1016/j.enconman.2018.03.081> (2018).
- Ouafia, F., Ahmed, A., Hassane, M. & Soufiane, G. Optimized MPPT for aero-generator system built on autonomous squirrel cage generators using feed-forward neural network. *Int. J. Renew. Energy Res.-IJRES*. **13** (3), 1134–1144. <https://doi.org/10.20508/ijrer.v13i3.14002.g8785> (2023).
- Al-Waeli, H. A. et al. Comparison of prediction methods of PV/T nanofluid and nano-PCM system using a measured dataset and artificial neural network. *Sol. Energy* **162**, 378–396. <https://doi.org/10.1016/j.solener.2018.01.026> (2018).
- Owusu-Nyarko, I., Elgenedy, M. A. & Ahmed, K. Combined Temperature and Irradiation Effects on the Open Circuit Voltage and Short Circuit Current Constants for Enhancing their Related PV-MPPT Algorithms. 2019 IEEE Conference on Power Electronics and Renewable Energy (CPERE), Aswan City, Egypt, 343–348 (2019).
- Ruhi, Z. C., Korhan, K., Mariacristina, R., Abdelhakim, B. & Abdelfatah, N. A. Comparative analysis of P&O, IC and supertwisting sliding mode based MPPT methods for PV and fuel cell sourced hybrid system. *Int. J. Renew. Energy Res.-IJRES*. **13** (3), 1431–1442. <https://doi.org/10.20508/ijrer.v13i3.14550.g8815> (2023).
- Swaminathan, B. et al. Performance optimization of an interleaved boost converter with water cycle optimized PO algorithm-based MPPT for the applications of solar-powered E-vehicles. *Int. J. Renew. Energy Res.-IJRES*. **14** (2), 248–260. <https://doi.org/10.20508/ijrer.v14i2.14277.g8887> (2024).
- Zakaria, M. Design of high-performance fuzzy-predictive controllers for a photovoltaic/battery pumping system. *Int. J. Renew. Energy Res.-IJRES*. **13** (1), 442–453. <https://doi.org/10.20508/ijrer.v13i1.13587.g8702> (2023).

34. Keerthi, S. S., Balamurugan, R., Karuppiah, N. & Two Stage, P. V. Generation system with novel control strategy to improve grid integrating capabilities during partial shading conditions. *Int. J. Renew. Energy Res.-IJRER*. **14** (2), 437–449. <https://doi.org/10.20508/ijrer.v14i2.14423.g8903> (2024).
35. Abdessamad, B., Mohammed, F., Reda, R. & Khalid, C. Implementation of genetic algorithm to generate backstepping controller's gains for MPPT of partially shaded photovoltaic panels. *Int. J. Renew. Energy Res.-IJRER*. **14** (3), 526–537. <https://doi.org/10.20508/ijrer.v14i3.14360.g8919> (2024).
36. Al-Dhaifallah, M., Nassef, A. M., Rezk, H. & Nisar, K. S. Optimal parameter design of fractional order control based INC-MPPT for PV system. *Sol. Energy* **159**, 650–664. <https://doi.org/10.1016/j.solener.2017.11.040> (2018).
37. Ferdous, S. M., Shafiullah, G. M., Oninda, M. A. M., Shoeb, M. A. & Jamal, T. Close loop compensation technique for high performance MPPT using ripple correlation control. *2017 Australasian Universities Power Engineering Conference (AUPEC)*, Melbourne, 1–6 (2017).
38. Ali, A. I. M. et al. An enhanced P&O MPPT algorithm with concise search area for Grid-Tied PV systems. *IEEE Access*. **11**, 79408–79421. <https://doi.org/10.1109/ACCESS.2023.3298106> (2023).
39. Hong, V. P. N., Thanh, T. H. & Van, T. N. Comparative efficiency assessment of MPPT algorithms in photovoltaic systems. *Int. J. Renew. Energy Res.-IJRER*. **12** (4), 2061–2067. <https://doi.org/10.20508/ijrer.v12i4.13481.g8565> (2022).
40. Sarika, P. E., Josephkutty, J., Sheik, M. & Shiny, P. A. Novel hybrid maximum power point tracking technique with zero oscillation based on P&O algorithm. *Int. J. Renew. Energy Res.-IJRER* **10** (4), 1962–1973. <https://doi.org/10.20508/ijrer.v10i4.11502.g8096> (2020).
41. Nirmal, K. P., Rupendra, K. P., Sushabhan, C. & Sudhakar, B. T. Frequency locked loop-based control algorithm with enhanced second-order generalized integrator for PV-battery integrated system to improve power quality. *Int. J. Renew. Energy Res.-IJRER*. **14** (1), 155–165. <https://doi.org/10.20508/ijrer.v14i1.14241.g8870> (2024).
42. Maniraj, B., Peer, F. A. & Stella, M. PV output power enhancement using meta-heuristic crow search algorithm under uniform and shading condition. *Int. J. Renew. Energy Res.-IJRER*. **13** (3), 117–124. <https://doi.org/10.20508/ijrer.v13i1.13512.g8666> (2023).
43. Hind, E. et al. Based on high gain observer for photovoltaic system. *Int. J. Renew. Energy Res.-IJRER*. **13** (3), 1332–1341. <https://doi.org/10.20508/ijrer.v13i3.14190.g8804> (2023).
44. Mohamed, A. Z., Badreddine, K., Fatma, B. S. & Hsan, H. A. A comparative study of distinct advanced MPPT algorithms for a PV boost converter. *Int. J. Renew. Energy Res.-IJRER*. **11** (3), 1156–1165. <https://doi.org/10.20508/ijrer.v11i3.12079.g8282> (2021).
45. Maniraj, A., Peer, F. & Stella, M. PV output power enhancement using meta-heuristic crow search algorithm under uniform and shading condition. *Int. J. Renew. Energy Res.-IJRER*. **13** (3), 117–124. <https://doi.org/10.20508/ijrer.v13i1.13512.g8666> (2023).
46. Pradhan, R. & Subudhi, B. Double integral sliding mode MPPT control of a photovoltaic system. *IEEE Trans. Control Syst. Technol.* **24** (1), 285–292. <https://doi.org/10.1109/TCST.2015.2420674> (2016).
47. Singh, S., Saini, S., Gupta, S. K. & Kumar, R. Solar-PV inverter for the overall stability of power systems with intelligent MPPT control of DC-Link capacitor voltage. *Prot. Control Mod. Power Syst.* **8** (1), 1–20. <https://doi.org/10.1186/s41601-023-00285-y> (2023).
48. Rajeev, K., Sourav, D., Pavan, K., Sheetal, S. & Manoj, B. Multimachine stability enhancement with hybrid PSO-BFOA based PV-STATCOM. *Sustain. Comput. Inf. Syst.* **32**, 100615. <https://doi.org/10.1016/j.suscom.2021.100615> (2021).
49. Kumar, R. et al. Performance assessment of the two metaheuristic techniques and their hybrid for power system stability enhancement with PV-STATCOM. *Neural Comput. Appl.* **34**, 3723–3744. <https://doi.org/10.1007/s00521-021-06637-9> (2022).
50. Karima, B., Nedjoud, B., Mohamed, B., Benbouhenni, H. & Ilhami, C. Performance enhancement of a three-phase grid-connected PV inverter system using fractional-order integral sliding mode controls. *Energy Rep.* **11**, 3976–3994. <https://doi.org/10.1016/j.energy.2024.03.049> (2024).
51. Dabdouche, N. et al. Genetic algorithm-super-twisting technique for grid-connected PV system associate with filter. *Energy Rep.* **10**, 4231–4252. <https://doi.org/10.1016/j.egy.2023.10.074> (2023).
52. Meganathan, P., Meganathan, P., Sasi, C., Pugazhendiran, P. & Nammalvar, P. An e-BAS optimized d-q controller for grid voltage stability of single stage solar PVS with PQ disputes. *Int. J. Renew. Energy Res.-IJRER*. **13** (4), 1592–1603. <https://doi.org/10.20508/ijrer.v13i4.14057.g8837> (2023).
53. Ravindhar, B., Suresh & Mangu, B. Optimal coordinated voltage control in distribution system considering smart inverter interfaced solar PV penetration. *Int. J. Renew. Energy Res.-IJRER*. **14** (1), 38–47. <https://doi.org/10.20508/ijrer.v14i1.14362.g8854> (2024).
54. Debouché, N., Deffaf, B., Habib, B., Laid, Z. & Mosaad, M. I. Direct power control for three-level multifunctional voltage source inverter of PV systems using a simplified super-twisting algorithm. *Energies* **16**, 4103. <https://doi.org/10.3390/en16104103> (2023).
55. Naamane, D. et al. A new nonlinear control to improve the efficiency of the PV-SAPF system. *Energy Rep.* **11**, 3096–3116. <https://doi.org/10.1016/j.egy.2024.02.051> (2024).
56. Mehiri, A., Bettayeb, M. & Hamid, A. K. Fractional nonlinear synergetic control based MPPT algorithm for PV system. *2019 Advances in Science and Engineering Technology International Conferences (ASET), Dubai, United Arab Emirates*, 1–5. <https://doi.org/10.1109/ICASET.2019.8714527> (2019).
57. Nouredine, A. Combination of artificial neural network-based approaches to control a grid-connected photovoltaic source under partial shading condition. *Int. J. Renew. Energy Res.-IJRER*. **13** (2), 778–789. <https://doi.org/10.20508/ijrer.v13i2.13530.g8753> (2023).
58. Mao, M., Xu, Z., Yuan, Q. & Li, H. Current interharmonic prediction control based on MPC and Lyapunov for Grid-Connected PV system. *IEEE J. Emerg. Sel. Top. Power Electron.* **12** (3), 2686–2696. <https://doi.org/10.1109/JESTPE.2024.3384317> (2024).
59. Celik, O. & Teke, A. A hybrid MPPT method for grid connected photovoltaic systems under rapidly changing atmospheric conditions. *Electr. Power Syst. Res.* **152**, 194–210. <https://doi.org/10.1016/j.epsr.2017.07.011> (2017).
60. Imane, A. A., Elmostafa, E. & Mohamed, B. Open-circuit and short-circuit fault diagnosis and fault tolerant strategy for non-isolated three-level boost DC-DC converters for photovoltaic energies applications. *Int. J. Renew. Energy Res.-IJRER* **13** (4), 1669–1679. <https://doi.org/10.20508/ijrer.v13i4.14101.g8844> (2023).
61. Kamaruzzaman, S., Ghaith, Y. A. & Alaa, M. Energy efficiency enhancement of solar-powered PV cooling system with PCM storage tank. *Int. J. Renew. Energy Res.-IJRER*. **13** (4), 1661–1668. <https://doi.org/10.20508/ijrer.v13i4.14123.g8843> (2023).
62. Arunachala, U. C., Manoj, T. K. & Varun, K. Ergo enviro economic analysis of photovoltaic module with multiple passive thermal management techniques. *Int. J. Renew. Energy Res.-IJRER*. **13** (2), 718–729. <https://doi.org/10.20508/ijrer.v13i2.13691.g8744> (2023).
63. Murat, A., Emrah, D. & Ramazan, B. A coordinated EV charging scheduling containing PV system. *Int. J. Smart Grid-ijSmartGrid*. **6** (3), 65–71. <https://doi.org/10.20508/ijsmartgrid.v6i3.252.g240> (2022).
64. Guerra, M., Araújo, F., Dhimish, M. & Vieira, R. G. Assessing maximum power point tracking intelligent techniques on a PV system with a Buck-Boost converter. *Energies* **14** (22), 7453. <https://doi.org/10.3390/en14227453> (2021).
65. Li, X., Wen, H. & Hu, Y. Evaluation of different maximum power point tracking (MPPT) techniques based on practical meteorological data. In *2016 IEEE International Conference on Renewable Energy Research and Applications (ICRERA), Birmingham*, 696–701 (2016).
66. Serrano-Guerrero, X., González-Romero, J., Cárdenas-Carangui, X. & Escrivá-Escrivá, G. Improved variable step size P&O MPPT algorithm for PV systems. In *2016 51st International Universities Power Engineering Conference (UPEC), Coimbra* 1–6 (2016).

67. Tang, S. Q. et al. An enhanced MPPT method combining fractional-order and fuzzy logic control. *IEEE J. Photovolt.* **7**, 640–650 (2017).
68. Soon, T. K. & Mekhilef, S. A fast-converging MPPT technique for photovoltaic system under fast-varying solar irradiation and load resistance. *IEEE Trans. Ind. Inf.* **11** (1), 176–186. <https://doi.org/10.1109/TII.2014.2378231> (2015).
69. Tey, K. S. et al. Improved differential evolution-based MPPT algorithm using SEPIC for PV systems under partial shading conditions and load variation. *IEEE Trans. Ind. Inf.* **14** (10), 4322–4333. <https://doi.org/10.1109/TII.2018.2793210> (2018).
70. Ahmad, J., Spertino, F., Ciocia, A. & Di, L. P. A Maximum Power Point Tracker for module integrated PV systems under rapidly changing irradiance conditions. In *2015 IEEE 5th International Conference on Consumer Electronics-Berlin (ICCE-Berlin), Berlin, Germany* 519–520. <https://doi.org/10.1109/ICCE-Berlin.2015.7391327> (2015).

## Acknowledgements

This research was supported by King Khalid University, Research Project RGP.2/472/45.

## Author contributions

Conceptualization: Abdelkadir Belhadj Djilali, Elhadj Bounadja, Adil Yahdou, Habib Benboughenni methodology: Abdelkadir Belhadj Djilali, Adil Yahdou, Habib Benboughenni, Z.M.S. Elbarbary, Ilhami Colak, Saad F. Al-Gahtani software: Abdelkadir Belhadj Djilali, Elhadj Bounadja, Adil Yahdou, Habib Benboughenni validation: Abdelkadir Belhadj Djilali, Elhadj Bounadja, Adil Yahdou formal analysis: Abdelkadir Belhadj Djilali, Habib Benboughenni, Z.M.S. Elbarbary, Ilhami Colak, Saad F. Al-Gahtani investigation: Abdelkadir Belhadj Djilali, Habib Benboughenni, Z.M.S. Elbarbary, Ilhami Colak, Saad F. Al-Gahtani resources: Abdelkadir Belhadj Djilali, Elhadj Bounadja, Habib Benboughenni, Z.M.S. Elbarbary, Saad F. Al-Gahtani data curation: Abdelkadir Belhadj Djilali, Adil Yahdou, Habib Benboughenni, Z.M.S. Elbarbary, Ilhami Colak, Saad F. Al-Gahtani writing—original draft preparation: Abdelkadir Belhadj Djilali, Elhadj Bounadja, Adil Yahdou, Habib Benboughenni writing—review and editing: Abdelkadir Belhadj Djilali, Habib Benboughenni, Z.M.S. Elbarbary, Ilhami Colak, Saad F. Al-Gahtani visualization: Abdelkadir Belhadj Djilali, Habib Benboughenni, Z.M.S. Elbarbary, Ilhami Colak, Saad F. Al-Gahtani supervision: Habib Benboughenni, Z.M.S. Elbarbary, Ilhami Colak, Saad F. Al-Gahtani project administration: Abdelkadir Belhadj Djilali, Habib Benboughenni, Z.M.S. Elbarbary, Ilhami Colak, Saad F. Al-Gahtani funding acquisition: Habib Benboughenni, Z.M.S. Elbarbary, Ilhami Colak, Saad F. Al-Gahtani All authors have read and agreed to the published version of the manuscript.

## Declarations

### Competing interests

The authors declare no competing interests.

### Additional information

**Correspondence** and requests for materials should be addressed to H.B.

**Reprints and permissions information** is available at [www.nature.com/reprints](http://www.nature.com/reprints).

**Publisher's note** Springer Nature remains neutral with regard to jurisdictional claims in published maps and institutional affiliations.

**Open Access** This article is licensed under a Creative Commons Attribution-NonCommercial-NoDerivatives 4.0 International License, which permits any non-commercial use, sharing, distribution and reproduction in any medium or format, as long as you give appropriate credit to the original author(s) and the source, provide a link to the Creative Commons licence, and indicate if you modified the licensed material. You do not have permission under this licence to share adapted material derived from this article or parts of it. The images or other third party material in this article are included in the article's Creative Commons licence, unless indicated otherwise in a credit line to the material. If material is not included in the article's Creative Commons licence and your intended use is not permitted by statutory regulation or exceeds the permitted use, you will need to obtain permission directly from the copyright holder. To view a copy of this licence, visit <http://creativecommons.org/licenses/by-nc-nd/4.0/>.

© The Author(s) 2025